FOUNDATIONS ADVANCES

ISSN 2053-2733

Pairwise correlations in layered close-packed structures

P. M. Riechers,* D. P. Varn* and J. P. Crutchfield*

Complexity Sciences Center and Physics Department, University of California, One Shields Avenue, Davis, California 95616, USA. *Correspondence e-mail: pmriechers@ucdavis.edu, dpv@complexmatter.org, chaos@ucdavis.edu

Received 18 July 2014
Accepted 14 March 2015

Edited by D. A. Keen, STFC Rutherford Appleton Laboratory, UK

Keywords: X-ray diffraction; planar disorder; stacking fault; z-transformation; spectral decomposition; pair distribution function.

Given a description of the stacking statistics of layered close-packed structures in the form of a hidden Markov model, analytical expressions are developed for the pairwise correlation functions between the layers. These may be calculated analytically as explicit functions of model parameters or the expressions may be used as a fast, accurate and efficient way to obtain numerical values. Several examples are presented, finding agreement with previous work as well as deriving new relations.

1. Introduction

There has long been an interest in planar defects or stacking faults in crystals (Hendricks & Teller, 1942; Wilson, 1942). With the recent realization of the technological import of many materials prone to stacking faults – graphene (Castro Neto *et al.*, 2009; Geim & Grigorieva, 2013) and SiC (Zekentes & Rogdakis, 2011) being but two well known examples – that interest has only grown. Since stacking faults shift an entire layer of atoms, it is not unexpected that they can profoundly affect material properties. Many of these materials have more than one stable stacking configuration and additionally many metastable ones can exist (Sebastian & Krishna, 1994), as well as many stacking configurations that show varying amounts of disorder. Thus, understanding stacking faults, perhaps as a prelude to controlling their kind and placement, presents a significant, but compelling challenge.

Disordered layered materials are often studied *via* the pairwise correlations between layers, as these correlations are experimentally accessible from the Fourier analysis of a diffraction pattern (Estevez-Rams, Martinez *et al.*, 2001; Estevez-Rams, Penton-Madrigual *et al.*, 2001; Varn *et al.*, 2002, 2013*a*), or directly from simulation studies (Kabra & Pandey, 1988, 1995; Shrestha & Pandey, 1996*a*,*b*, 1997; Shrestha *et al.*, 1996; Varn & Crutchfield, 2004). Such studies yield important insights into the structural organization of materials. For example, Kabra & Pandey (1988) were able to show that a model of the $2H \Rightarrow 6H$[1] transformation in SiC could retain long-range order even as the short-range order was reduced. Tiwary & Pandey (2007) calculated the size of domains in a model of randomly faulted close-packed structures (CPSs) by calculating the (exponential) decay rate of pairwise correlation functions between layers. Recently Estevez-Rams *et al.* (2008) derived analytical expressions for the correlation functions for CPSs that contained both random growth and deformation faults, and Beyerlein *et al.* (2011) demonstrated

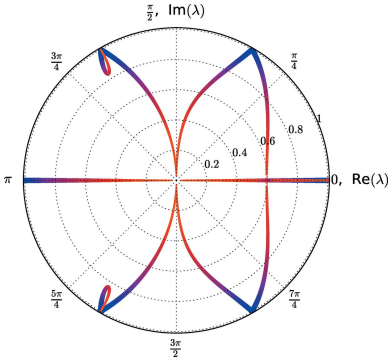

[1] We will use the Ramsdell notation (Ortiz *et al.*, 2013; Sebastian & Krishna, 1994) to describe well known crystalline stacking structures.

Table 1
A number of abbreviations are extensively used in the text and, as a convenience for the reader, they are tabulated here.

CF	Correlation function	§2.1
CPS	Close-packed structure	§1
GM	Golden Mean (process)	§2.2
HMM	Hidden Markov model	§1
IID	Independent and identically distributed (process)	§5.1
ML	Modular layer	§2
RGDF	Random growth and deformation fault (process)	§5.2
SF	Stacking fault	§5.2
SFSF	Shockley–Frank stacking fault (process)	§5.3
SSC	Simple state cycle	§3.2
TM	Transition matrix	§2.2

that correlation functions in finite-sized face-centered cubic crystals depend not only on the kind and amount of faulting, but additionally on their placement.

Beyond the study of layered materials, pairwise correlation information, in the form of *pair distribution functions*, has recently attracted significant attention (Egami & Billinge, 2013). However, as useful as the study of pairwise correlation information is, it does *not* provide a complete description of the specimen. Indeed, it has long been known that very different atomic arrangements of atoms can reproduce the same pair distribution function, although there has been recent progress in reducing this degeneracy (Cliffe *et al.*, 2010). Nor are they in general suitable for calculating material properties, such as conductivities or compressibilities.

For crystalline materials, a complete description of the specimen comes in the form of its crystal structure, *i.e.*, the specification of the placement of all the atoms within the unit cell, coupled with the description of how the unit cells are spatially related to each other, commonly referred to as the lattice. The mathematical structure of the theory, which has been called *classical crystallography* (Mackay, 1986), uses exact symmetries couched in the language of group theory. Determining these quantities for specimens and materials is of course the traditional purview of crystallography. For disordered materials, instead of using exact group symmetries, it has recently been suggested that the partial symmetries observed in these materials can be represented using semigroups. This new formalism, called *chaotic crystallography* (Varn & Crutchfield, 2015), employs information- and computation-theoretic measures to characterize and classify material structure. Chaotic crystallography provides a unified platform not only to calculate physical quantities of interest but also to give insight into their physical structure. For layered materials, where there is but one axis of interest, namely the organization along the stacking direction, the appropriate mathematical framework for this formalism has been identified (Varn *et al.*, 2002, 2007, 2013*a*) as *computational mechanics* (Crutchfield & Young, 1989; Crutchfield, 2012). The mathematical entity that gives a compact, statistical description of the disordered material (along its stacking direction) is its ε-machine, a kind of hidden Markov model (HMM) (Rabiner, 1989; Elliot *et al.*, 1995). Chaotic crystallography also has the advantage of encompassing traditional crystal structures, so both ordered and disordered materials can be treated on the same footing in the same formalism.

It is our contention that an ε-machine describing a specimen's stacking includes all of the structural information necessary to calculate physical quantities that depend on the stacking statistics (Varn & Crutchfield, 2015). In the following, we demonstrate how pairwise correlation functions can be calculated either *analytically* or to a high degree of numerical certainty for an arbitrary HMM and, thus, for an arbitrary ε-machine. Previous researchers often calculated pairwise correlation functions for particular realizations of stacking configurations (Berliner & Werner, 1986; Kabra & Pandey, 1988; Shrestha & Pandey, 1997; Estevez-Rams, Martinez *et al.*, 2001; Varn *et al.*, 2013*a*) or from analytic expressions constructed for particular models (Tiwary & Pandey, 2007; Estevez-Rams *et al.*, 2008; Varn & Crutchfield, 2004). The techniques developed here, however, are the first generally applicable methods that do not rely on samples of a stacking sequence. The result delivers both an analytical solution and an efficient numerical tool. Additionally, by shifting the primary focus of study from the pair correlation functions to the HMM, new insights into the behavior of correlation functions, particularly their modes of decay to their asymptotic value, are obtained. While we will specialize to the case of CPSs for concreteness, the methods developed are extendable to other materials and stacking geometries.

Our development is organized as follows. In §2 we introduce nomenclature. In §3 we develop an algorithm to change between different representations of stacking sequences. In §4 we derive expressions, our main results, for the pairwise correlation functions between layers in layered CPSs. In §5 we consider several examples: namely, (i) a simple stacking process that represents the 3*C* crystal structure or a random stacking structure depending on the parameter choice, (ii) a stacking process that models random growth and deformation faults, and (iii) a stacking process inspired by recent experiments in 6*H*-SiC. And, in §6 we give our conclusions and directions for future work.

Additionally, we find it useful to introduce a number of abbreviations that may not be familiar to the reader. As an aid, these abbreviations have been compiled in Table 1 along with the section of the text where they are first defined.

2. Definitions and notations

We suppose the layered material is built up from identical sheets called *modular layers* (MLs) (Price, 1983; Ferraris *et al.*, 2008). The MLs are completely ordered in two dimensions and assume only one of three discrete positions, labeled A, B or C (Ashcroft & Mermin, 1976; Sebastian & Krishna, 1994). These represent the physical placement of each ML and are commonly known as the ABC notation (Ortiz *et al.*, 2013). We define the set of possible orientations in the ABC notation as $\mathcal{A}_{\rm P} = \{A, B, C\}$. We further assume that the MLs obey the same stacking rules as CPSs, namely that two adjacent layers may not have the same orientation; *i.e.*, stacking sequences AA, BB and CC are not allowed. Exploiting this constraint,

the stacking structure can be represented more compactly in the Hägg notation: one takes the transitions between MLs as being either cyclic, ($A \to B$, $B \to C$ or $C \to A$), and denoted as '+'; or anticyclic, ($A \to C$, $C \to B$ or $B \to A$), and denoted as '−'. The Hägg notation then gives the relative orientation of each ML to its predecessor. It is convenient to identify the usual Hägg notation '+' as '1' and '−' as '0'. Doing so, we define the set of possible relative orientations in the Hägg notation as $\mathcal{A}_{\rm H} = \{0, 1\}$. These two notations – *ABC* and Hägg – carry an identical message, up to an overall rotation of the specimen. Alternatively, one can say that there is freedom of choice in labeling the first ML. However, only the *ABC* sequences directly relate to structure factors for the specimen, making the *ABC* representation of the stacking structure the natural choice for calculating pairwise correlation quantities. Indeed, it will be shown that the spectral decomposition of the *ABC* transition matrix directly corresponds to modes of the correlation functions relevant to diffraction patterns, whereas the same is not true for the Hägg representation.

2.1. Correlation functions

Let us define three statistical quantities, $Q_{\rm c}(n)$, $Q_{\rm a}(n)$ and $Q_{\rm s}(n)$ (Yi & Canright, 1996): the pairwise *correlation functions* (CFs) between MLs, where 'c', 'a' and 's' stand for cyclic, anticyclic and same, respectively. $Q_{\rm c}(n)$ is the probability that any two MLs at a separation of n are cyclically related. $Q_{\rm a}(n)$ and $Q_{\rm s}(n)$ are defined in a similar fashion.[2] Since these are probabilities: $0 \leq Q_\xi(n) \leq 1$, where $\xi \in \{\rm c, a, s\}$. Additionally, at each n it is clear that $\sum_\xi Q_\xi(n) = 1$. Notice that the CFs are defined in terms of the *ABC* notation.

2.2. Representing layer stacking as a hidden process

We chose to represent a stacking sequence as the output of a discrete-step, discrete-state HMM. A HMM Γ is an ordered tuple $\Gamma = (\mathcal{A}, \mathbb{S}, \mu_0, \mathbf{T})$, where $\mathcal{A}$ is the set of symbols that one observes as the HMM's output, often called an alphabet, $\mathbb{S}$ is a finite set of M internal states, μ_0 is an initial state probability distribution, and $\mathbf{T}$ is a set of matrices that give the probability of making a transition between the states while outputting one of the symbols in $\mathcal{A}$. These transition probability matrices or more simply *transition matrices* (TMs) (Paz, 1971; Karlin & Taylor, 1975) are usually written:

$$\mathcal{T}^{[s]} = \begin{bmatrix} \Pr(s, \mathsf{S}_1|\mathsf{S}_1) & \Pr(s, \mathsf{S}_2|\mathsf{S}_1) & \dots & \Pr(s, \mathsf{S}_M|\mathsf{S}_1) \\ \Pr(s, \mathsf{S}_1|\mathsf{S}_2) & \Pr(s, \mathsf{S}_2|\mathsf{S}_2) & \dots & \Pr(s, \mathsf{S}_M|\mathsf{S}_2) \\ \vdots & \vdots & \ddots & \vdots \\ \Pr(s, \mathsf{S}_1|\mathsf{S}_M) & \Pr(s, \mathsf{S}_2|\mathsf{S}_M) & \dots & \Pr(s, \mathsf{S}_M|\mathsf{S}_M) \end{bmatrix},$$

where $s \in \mathcal{A}$ and $\mathsf{S}_1, \mathsf{S}_2, \ldots, \mathsf{S}_M \in \mathbb{S}$.

For a number of purposes it is convenient to work directly with the internal-state TM; denote it $\mathcal{T}$. This is the matrix of state transition probabilities regardless of symbol, given by the sum of the symbol-labeled TMs: $\mathcal{T} = \sum_{x\in\mathcal{A}} \mathcal{T}^{[x]}$. For example, the ensemble internal-state distribution evolves according to $\langle \boldsymbol{\mu}_1| = \langle \boldsymbol{\mu}_0|\mathcal{T}$. Or, more generally, $\langle \boldsymbol{\mu}_L| = \langle \boldsymbol{\mu}_0|\mathcal{T}^L$. (In this notation, state distributions are row vectors.) In another use, one finds the stationary-state probability distribution:

$$\langle \boldsymbol{\pi}| = [\Pr(\mathsf{S}_1)\ \Pr(\mathsf{S}_2)\ \dots\ \Pr(\mathsf{S}_M)],$$

as the left eigenvector of $\mathcal{T}$ normalized in probability:

$$\langle \boldsymbol{\pi}| = \langle \boldsymbol{\pi}|\mathcal{T}. \qquad (1)$$

The probability of any finite-length sequence of symbols can be computed exactly from these objects using linear algebra. In particular, a length-L 'word' $w = s_0 s_1 \ldots s_{L-1} \in \mathcal{A}^L$, where $\mathcal{A}^L$ is the set of length-L sequences, has the stationary probability:

$$\begin{aligned} \Pr(w) &= \langle \boldsymbol{\pi}|\mathcal{T}^{[w]}|\mathbf{1}\rangle \\ &= \langle \boldsymbol{\pi}|\mathcal{T}^{[s_0]}\mathcal{T}^{[s_1]}\ldots\mathcal{T}^{[s_{L-1}]}|\mathbf{1}\rangle, \end{aligned}$$

where $|\mathbf{1}\rangle$ is the column vector of all ones.

As a useful convention, we will use bras $\langle\cdot|$ to denote row vectors and kets $|\cdot\rangle$ to denote column vectors. On the one hand, any object closed by a bra on the left and ket on the right is a scalar and commutes as a unit with anything. On the other hand, a ket–bra $|\cdot\rangle\langle\cdot|$ has the dimensions of a square matrix. More explanation can be found in Appendix *A*.

To help familiarize the reader with TMs as they will be employed in the examples of §5, and to make a very useful connection to automata theory (Hopcroft & Ullman, 1979), we now develop these ideas using a simple pedagogical example. Let us consider a CPS stacked according to the *Golden Mean* (GM) process (Crutchfield & Feldman, 2003). The GM process has been previously treated in the context of CPSs in Varn (2013*b*). The GM process is generically defined as follows: any sequence is allowed as long as there are no consecutive 0's. This is accomplished by examining the previous observed symbol: if it is 1, then the next symbol in the sequence is either 0 or 1 with equal probability; if it is 0, then the next symbol is necessarily 1.[3] Thus, when scanning a sequence there are two possible states corresponding to the above two conditions. Let us call these states $\mathcal{U}$ (next symbol is a 0 or 1 with equal probability) and $\mathcal{V}$ (next symbol is a 1). And so, we say $\mathbb{S} = \{\mathcal{U}, \mathcal{V}\}$. The two 2-by-2 TMs for this process – one for each symbol in the alphabet – are given by

[2] As yet, there is no consensus on notation for these quantities. Warren (1969) uses P_m^0, P_m^+ and P_m^-; Kabra & Pandey (1988) call these $P(m)$, $Q(m)$ and $R(m)$; and Estevez-Rams *et al.* (2008) use $P_0(\Delta)$, $P_{\rm f}(\Delta)$ and $P_{\rm b}(\Delta)$. Since we prefer to reserve the symbol 'P' for other probabilities previously established in the literature, here and elsewhere we follow the notation of Yi & Canright (1996), with a slight modification of replacing '$Q_{\rm r}(n)$' with '$Q_{\rm a}(n)$'.

[3] The alert reader may object that there isn't any inherent prohibition against consecutive 0's appearing in the stacking sequence of CPSs. She is quite right. While there is no general prohibition, it may be that in a *particular* specimen, whether by accident, by some natural as yet undiscovered mechanism or by the design of an experimentalist, the 00 sequence never appears. This should be reflected in the HMM. Additionally, the reader may object that rotating the specimen by 60° about the stacking direction will exchange all 0's and 1's, making such sequence prohibitions spurious. Indeed, for simple CPSs, $0 \Leftrightarrow 1$ is a good symmetry. [See Varn & Canright (2001) for a discussion.] While a physical rotation of the specimen doesn't alter the physical stacking, it can alter the details of how the stacking sequence is labeled, and this *is* reflected in the HMM. In any event, the details of the GM process are not relevant to our overall theoretical development, and the prohibition of the 00 sequence just serves to create a simple HMM that is both nontrivial and easy to analyze.

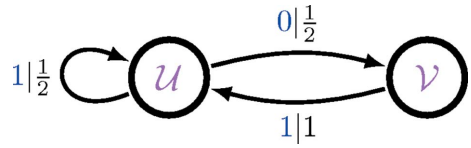

Figure 1
The GM process written as a Hägg-machine. The circles indicate states, and the arcs between them are transitions, labeled by $s|p$, where s is the symbol emitted upon transition and p is the probability of making such a transition.

$$\mathsf{T}^{[0]} = \begin{bmatrix} 0 & \frac{1}{2} \\ 0 & 0 \end{bmatrix} \quad \text{and} \quad \mathsf{T}^{[1]} = \begin{bmatrix} \frac{1}{2} & 0 \\ 1 & 0 \end{bmatrix}.$$

The GM process has internal-state TM:

$$\mathsf{T} = \mathsf{T}^{[0]} + \mathsf{T}^{[1]} = \begin{bmatrix} \frac{1}{2} & \frac{1}{2} \\ 1 & 0 \end{bmatrix}.$$

The asymptotic state probabilities are found by direct application of equation (1) and are found to be $\langle \boldsymbol{\pi}_{\mathrm{H}}| = [\frac{2}{3}\ \frac{1}{3}]$.

Thus, a more formal definition of the GM process is given as $\Gamma^{(\mathrm{H})}_{\mathrm{GM}} = (\mathcal{A}, \mathbb{S}, \mu_0, \mathbf{T}) = (\{0,1\}, \{\mathcal{U}, \mathcal{V}\}, [\frac{2}{3}\frac{1}{3}], \{\mathsf{T}^{[0]}, \mathsf{T}^{[1]}\})$.[4] HMMs are often conveniently depicted as a *finite-state automaton* (Hopcroft & Ullman, 1979), a kind of labeled directed graph. For example, the labeled directed graph that represents the HMM for the GM process is shown in Fig. 1. When the finite-state automaton representing the HMM is given in terms of the Hägg notation (as is done here), we will call that the *Hägg-machine* for that process.

Thus, if the MLs of a specimen were stacked according to the GM process, that would mean that sequences like 00 are never observed in that specimen. Alternatively, this can be restated in the *ABC* notation: sequences of the form *ACB*, *CBA* and *BAC* are not observed in that specimen. In the next section we show how to rewrite any Hägg-machine as a finite-state automaton in the *ABC* notation, which we will call the *ABC-machine*. This is the necessary mathematical object required to calculate CFs and will be used extensively in our theoretical development (§4).

3. Expanding the Hägg-machine to the *ABC*-machine

While simulation studies (Varn & Crutchfield, 2004) and ε-machine spectral reconstruction (Varn *et al.*, 2002, 2007, 2013*a*,*b*) express stacking structure in terms of the Hägg-machine, our theoretical methods developed in §4 require that it be re-expressed in terms of the *ABC*-machine. This section is devoted to detailing techniques to do just that. We give a graphical procedure for expanding the Hägg-machine into the *ABC*-machine (§3.1) and then provide an algebraically equivalent algorithm (§3.3). We note that this expansion procedure is *not* unique and can vary up to an overall rearrangement of the columns and rows of the resulting *ABC*-machine TM. This difference, of course, does not alter the results of calculations of physical quantities.

3.1. Graphical expansion method

Recall that the Hägg notation and the *ABC* notation are equivalent representations of the stacking structure, up to an overall rotation of the crystal. Stated alternatively, in the Hägg notation, there is an ambiguity concerning the orientation of each ML – it could be either *A*, *B* or *C*. To account for this degeneracy, when we transform to the *ABC* representation, we triple the size of the Hägg-machine. As a first step, one writes down three states for each state found in the Hägg-machine, but not the transitions between them. To distinguish among these new states of the triplet, label each with a superscript (*A*, *B* or *C*) indicating the last ML added to arrive at that state. Symbolically, this is stated:

$$\{S_i\} \overset{\text{Hägg to } ABC}{\Longrightarrow} \{\mathcal{S}_i^{[A]}, \mathcal{S}_i^{[B]}, \mathcal{S}_i^{[C]}\}.$$

Transitions between states on the *ABC*-machine still respect the same state-labeling scheme as on the Hägg-machine (explained below), but now they store the ML information. Transitions between states on the Hägg-machine that were labeled with 1 advance the stacking sequence cyclically (*i.e.*, $A \to B \to C \to A$) and the corresponding transitions on the *ABC*-machine reflect this by taking the ML label on the initial state and advancing it cyclically. In a completely analogous way, transitions labeled 0 on the Hägg-machine advance the states on the *ABC*-machine in an anticyclical fashion (*i.e.*, $A \to C \to B \to A$).

Continuing our GM process example, let us write out the six ($= 3 \times 2$) states labeled with superscripts to distinguish them. This is done in Fig. 2(*a*). [It does not matter in what order these states are labeled. The scheme chosen in Fig. 2(*a*) turns out to be convenient given the state-to-state transition structure of the final *ABC*-machine, but any arrangement is satisfactory.] The transitions between the states on the *ABC*-machine preserve the labeling scheme of the original Hägg-machine. That is, if in the original Hägg-machine there is transition $\mathsf{S}_i \xrightarrow{s|p} \mathsf{S}_j$, then there must be *three* similar transitions on the *ABC*-machine of the form $\mathcal{S}_i^{[x]} \xrightarrow{x'|p} \mathcal{S}_j^{[x']}$, with $x, x' \in \{A, B, C\}$. Additionally, the transitions on the *ABC*-machine corresponding to the transitions on the Hägg-machine have the same conditional probability.

Let us consider the self-state transition on the Hägg-machine shown in Fig. 1: $\mathcal{U} \xrightarrow{1|\frac{1}{2}} \mathcal{U}$. Since the corresponding transitions on the *ABC*-machine still respect the state-labeling scheme, the self-loop on $\mathcal{U}$ only induces transitions among the $\mathcal{U}^{[x]}$. Since a 1 advances the stacking sequence cyclically, the appropriate transitions are

[4] Here and in the examples of §5, we take the stationary-state probability distribution $\boldsymbol{\pi}$ as the initial probability state distribution μ_0, as we are interested for now in stationary behavior.

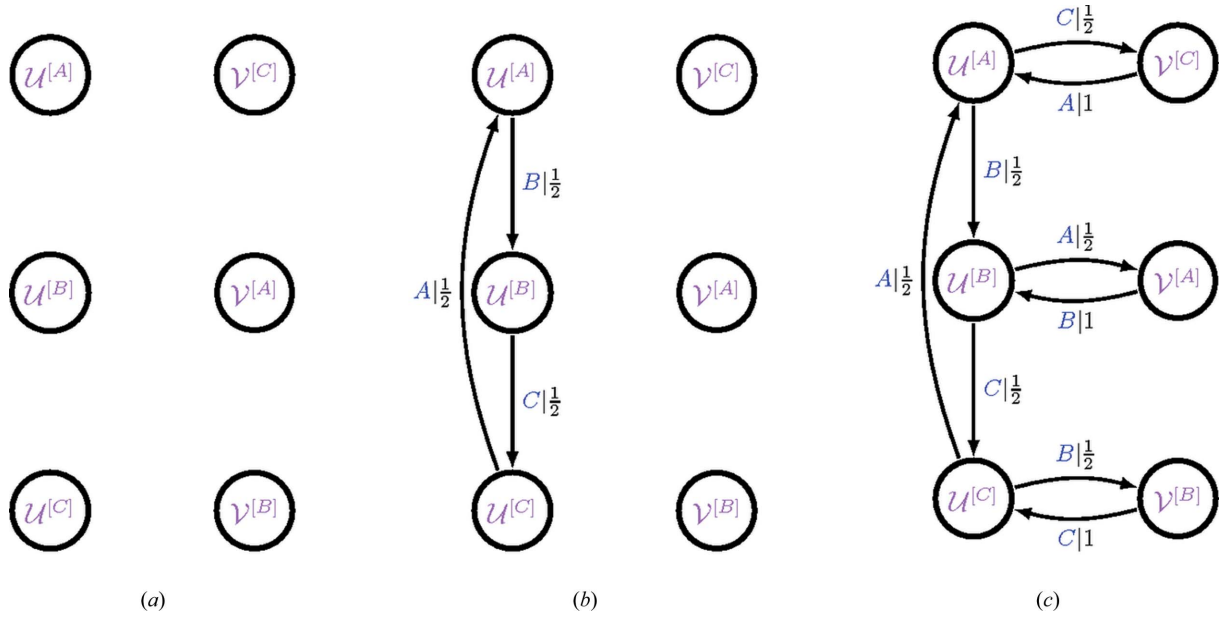

Figure 2
The steps to graphically expand the Hägg-machine to the ABC-machine demonstrated using the GM process. (*a*) The two states of Hägg-machine shown in Fig. 1 are increased to six, as shown. (*b*) The self-state transition $\mathcal{U} \overset{1|\frac{1}{2}}{\rightarrow} \mathcal{U}$ of the Hägg-machine now becomes three transitions among the $\mathcal{U}^{[x]}$ of the ABC-machine. (*c*) The remaining transitions of the Hägg-machine are expanded in a similar fashion (see text), resulting in the ABC-machine for the GM process.

$$\mathcal{U}^{[A]} \overset{B|\frac{1}{2}}{\longrightarrow} \mathcal{U}^{[B]}$$
$$\mathcal{U}^{[B]} \overset{C|\frac{1}{2}}{\longrightarrow} \mathcal{U}^{[C]}$$
$$\mathcal{U}^{[C]} \overset{A|\frac{1}{2}}{\longrightarrow} \mathcal{U}^{[A]}.$$

This is illustrated in Fig. 2(*b*). Applying the same procedure to the other transitions on the Hägg-machine, *i.e.*, $\mathcal{U} \overset{0|\frac{1}{2}}{\longrightarrow} \mathcal{V}$ and $\mathcal{V} \overset{1|1}{\longrightarrow} \mathcal{U}$, results in the completely expanded ABC-machine, and this is shown in Fig. 2(*c*).

We are now able to write down the stacking process for the GM process from its expanded graph, Fig. 2(*c*). First, we note that the alphabet is ternary: $\mathcal{A}_{\rm P} = \{A, B, C\}$. Second, there are six states on the ABC-machine, *i.e.*, $\mathcal{S} = \{\mathcal{U}^{[A]}, \mathcal{U}^{[B]}, \mathcal{U}^{[C]}, \mathcal{V}^{[A]}, \mathcal{V}^{[B]}, \mathcal{V}^{[C]}\}$. Ordering the states as above, the TMs may be directly constructed from the expanded graph, and are given by

$$\mathcal{T}^{[A]} = \begin{bmatrix} 0 & 0 & 0 & 0 & 0 & 0 \\ 0 & 0 & 0 & \frac{1}{2} & 0 & 0 \\ \frac{1}{2} & 0 & 0 & 0 & 0 & 0 \\ 0 & 0 & 0 & 0 & 0 & 0 \\ 0 & 0 & 0 & 0 & 0 & 0 \\ 1 & 0 & 0 & 0 & 0 & 0 \end{bmatrix}, \quad \mathcal{T}^{[B]} = \begin{bmatrix} 0 & \frac{1}{2} & 0 & 0 & 0 & 0 \\ 0 & 0 & 0 & 0 & 0 & 0 \\ 0 & 0 & 0 & 0 & \frac{1}{2} & 0 \\ 0 & 1 & 0 & 0 & 0 & 0 \\ 0 & 0 & 0 & 0 & 0 & 0 \\ 0 & 0 & 0 & 0 & 0 & 0 \end{bmatrix}$$

and

$$\mathcal{T}^{[C]} = \begin{bmatrix} 0 & 0 & 0 & 0 & 0 & \frac{1}{2} \\ 0 & 0 & \frac{1}{2} & 0 & 0 & 0 \\ 0 & 0 & 0 & 0 & 0 & 0 \\ 0 & 0 & 0 & 0 & 0 & 0 \\ 0 & 0 & 1 & 0 & 0 & 0 \\ 0 & 0 & 0 & 0 & 0 & 0 \end{bmatrix}.$$

As before, the internal-state TM is simply the sum of the symbol-specific TMs, given by $\mathcal{T} = \mathcal{T}^{[A]} + \mathcal{T}^{[B]} + \mathcal{T}^{[C]}$. For the GM process this turns out to be

$$\mathcal{T} = \begin{bmatrix} 0 & \frac{1}{2} & 0 & 0 & 0 & \frac{1}{2} \\ 0 & 0 & \frac{1}{2} & \frac{1}{2} & 0 & 0 \\ \frac{1}{2} & 0 & 0 & 0 & \frac{1}{2} & 0 \\ 0 & 1 & 0 & 0 & 0 & 0 \\ 0 & 0 & 1 & 0 & 0 & 0 \\ 1 & 0 & 0 & 0 & 0 & 0 \end{bmatrix}.$$

For completeness, the HMM for the GM process *in terms of the physical stacking of MLs* is $\Gamma^{(\rm P)}_{\rm GM} = (\mathcal{A}, \mathbb{S}, \mu_0, \mathbf{T}) = (\{A, B, C\}, \{\mathcal{U}^{[A]}, \mathcal{U}^{[B]}, \mathcal{U}^{[C]}, \mathcal{V}^{[A]}, \mathcal{V}^{[B]}, \mathcal{V}^{[C]}\}, \frac{1}{9}[2\,2\,2\,1\,1\,1], \{\mathcal{T}^{[A]}, \mathcal{T}^{[B]}, \mathcal{T}^{[C]}\})$. It is from such ABC representations that we will make direct connection to the CFs in §4.

3.2. Mixing and nonmixing state cycles

Observe Fig. 2(*c*)'s directed graph is *strongly connected* – any state is accessible from any other state in a finite number of transitions. It should be apparent that this need not have been the case. In fact, in this example connectivity is due to the presence of the self-state transition $\mathcal{U} \overset{1}{\longrightarrow} \mathcal{U}$. The latter guarantees a strongly connected expanded graph. Had this transition been absent on the Hägg-machine, such that there were only transitions of the form $\mathcal{U} \overset{0}{\longrightarrow} \mathcal{V}$ and $\mathcal{V} \overset{1}{\longrightarrow} \mathcal{U}$, the expansion would have yielded a graph with three distinct, unconnected components. Only one of these graphs would be physically manifest. It is sufficient to take just one component, arbitrarily assign an A, B or C to an arbitrary state on that component, and then replace all of the $\{0, 1\}$ transitions with the appropriate $\{A, B, C\}$ transitions, as done above.

To determine whether the expansion process on a Hägg-machine results in a strongly connected graph, one can examine the set of *simple state cycles* (SSCs) and calculate the *winding number* for each. An SSC is defined analogous to a *causal state cycle* (Varn *et al.*, 2013*a*) on an ε-machine as a 'finite, closed, nonself-intersecting, symbol-specific path' along the graph. The winding number W for an SSC on a Hägg-machine is similar to the parameter Δ previously defined by Yi & Canright (1996) and the *cyclicity* (C) (Dornberger-Schiff & Schmittler, 1971) for a polytype of a CPS. The winding number differs from cyclicity as the former is not divided by the period of the cycle. We define the winding number for an SSC as

$$W^{\mathrm{SSC}} = n_1 - n_0,$$

where n_1 and n_0 are the number of 1's and the number of 0's encountered traversing the SSC, respectively. We call those SSCs *mixing* if $W^{\mathrm{SSC}}(\mathrm{mod}\,3) \neq 0$, and *nonmixing* if $W^{\mathrm{SSC}}(\mathrm{mod}\,3) = 0$. If there is at least one mixing SSC on the Hägg-machine, then the expanded ABC-machine will be strongly connected. For example, there are two SSCs on the Hägg-machine for the GM process: $[\mathcal{U}]$ and $[\mathcal{U}\mathcal{V}]$.[5] The winding number for each is given by $W^{[\mathcal{U}]} = 1 - 0 = 1$ and $W^{[\mathcal{U}\mathcal{V}]} = 1 - 1 = 0$. Since $W^{[\mathcal{U}]} \neq 0$ and $[\mathcal{U}]$ is thus a mixing SSC, the Hägg-machine for the GM process will expand into a strongly connected ABC-machine. Let us refer to those Hägg-machines with at least one mixing SSC as *mixing Hägg-machines* and those that do not as *nonmixing Hägg-machines* and similarly for the corresponding ABC-machines. We find that mixing Hägg-machines, and thus mixing ABC-machines, are far more common than nonmixing ones and that the distinction between the two can have profound effects on the calculated quantities, such as the CFs and the diffraction pattern (Riechers *et al.*, 2014).

3.3. Rote expansion algorithm

To develop an algorithm for expansion, it is more convenient to change notation slightly. Let us now denote $\mathcal{S}$ as the set of hidden recurrent states in the ABC-machine, indexed by integer subscripts: $\mathcal{S} = \{\mathcal{S}_i : i = 1, \ldots, M_{\mathrm{P}}\}$, where $M_{\mathrm{P}} = |\mathcal{S}|$. Define the probability to transition from state $\mathcal{S}_i$ to state $\mathcal{S}_j$ on the symbol $x \in \mathcal{A}_{\mathrm{P}}$ as $\mathcal{T}^{[x]}_{i,j}$. Let's gather these state-to-state transition probabilities into an $M_{\mathrm{P}} \times M_{\mathrm{P}}$ matrix, referring to it as the *x-transition matrix* (x-TM) $\mathcal{T}^{[x]}$. Thus, there will be as many x-TMs as there are symbols in the alphabet of the ABC-machine, which is always $|\mathcal{A}_{\mathrm{P}}| = 3$ for CPSs.

As before, transitioning on symbol 1 has a threefold degeneracy in the ABC language, as it could imply any of the three transitions ($A \to B$, $B \to C$, or $C \to A$), and similarly for 0. Thus, each labeled edge of the Hagg-machine must be split into three distinct labeled edges of the ABC-machine. Similarly, each state of the Hägg-machine maps onto three distinct states of the ABC-machine. Although we have some flexibility in indexing states in the resulting ABC-machine, we establish consistency by committing to the following construction.[6]

If M_{H} is the number of states in the Hägg-machine, then $M_{\mathrm{P}} = 3\mathsf{M}_{\mathrm{H}}$ for mixing Hägg-machines. (The case of nonmixing Hägg-machines is treated afterwards.) Let the ith state of the Hägg-machine split into the $(3i-2)$-th through the $(3i)$-th states of the corresponding ABC-machine. Then, each labeled-edge transition from the ith to the jth states of the Hägg-machine maps into a 3-by-3 submatrix for each of the three labeled TMs of the ABC-machine as

$$\left\{\mathsf{T}^{[0]}_{ij}\right\} \overset{\text{Hägg to } ABC}{\Longrightarrow} \left\{\mathcal{T}^{[A]}_{3i-1,3j-2},\ \mathcal{T}^{[B]}_{3i,3j-1},\ \mathcal{T}^{[C]}_{3i-2,3j}\right\} \tag{2}$$

and

$$\left\{\mathsf{T}^{[1]}_{ij}\right\} \overset{\text{Hägg to } ABC}{\Longrightarrow} \left\{\mathcal{T}^{[A]}_{3i,3j-2},\ \mathcal{T}^{[B]}_{3i-2,3j-1},\ \mathcal{T}^{[C]}_{3i-1,3j}\right\}. \tag{3}$$

We can represent the mapping of equations (2) and (3) more visually with the following equivalent set of statements:

$$\begin{pmatrix} \mathcal{T}^{[A]}_{3i-2,3j-2} & \mathcal{T}^{[A]}_{3i-2,3j-1} & \mathcal{T}^{[A]}_{3i-2,3j} \\ \mathcal{T}^{[A]}_{3i-1,3j-2} & \mathcal{T}^{[A]}_{3i-1,3j-1} & \mathcal{T}^{[A]}_{3i-1,3j} \\ \mathcal{T}^{[A]}_{3i,3j-2} & \mathcal{T}^{[A]}_{3i,3j-1} & \mathcal{T}^{[A]}_{3i,3j} \end{pmatrix} = \begin{pmatrix} 0 & 0 & 0 \\ \mathsf{T}^{[0]}_{ij} & 0 & 0 \\ \mathsf{T}^{[1]}_{ij} & 0 & 0 \end{pmatrix}, \tag{4}$$

$$\begin{pmatrix} \mathcal{T}^{[B]}_{3i-2,3j-2} & \mathcal{T}^{[B]}_{3i-2,3j-1} & \mathcal{T}^{[B]}_{3i-2,3j} \\ \mathcal{T}^{[B]}_{3i-1,3j-2} & \mathcal{T}^{[B]}_{3i-1,3j-1} & \mathcal{T}^{[B]}_{3i-1,3j} \\ \mathcal{T}^{[B]}_{3i,3j-2} & \mathcal{T}^{[B]}_{3i,3j-1} & \mathcal{T}^{[B]}_{3i,3j} \end{pmatrix} = \begin{pmatrix} 0 & \mathsf{T}^{[1]}_{ij} & 0 \\ 0 & 0 & 0 \\ 0 & \mathsf{T}^{[0]}_{ij} & 0 \end{pmatrix} \tag{5}$$

and

$$\begin{pmatrix} \mathcal{T}^{[C]}_{3i-2,3j-2} & \mathcal{T}^{[C]}_{3i-2,3j-1} & \mathcal{T}^{[C]}_{3i-2,3j} \\ \mathcal{T}^{[C]}_{3i-1,3j-2} & \mathcal{T}^{[C]}_{3i-1,3j-1} & \mathcal{T}^{[C]}_{3i-1,3j} \\ \mathcal{T}^{[C]}_{3i,3j-2} & \mathcal{T}^{[C]}_{3i,3j-1} & \mathcal{T}^{[C]}_{3i,3j} \end{pmatrix} = \begin{pmatrix} 0 & 0 & \mathsf{T}^{[0]}_{ij} \\ 0 & 0 & \mathsf{T}^{[1]}_{ij} \\ 0 & 0 & 0 \end{pmatrix}, \tag{6}$$

which also yields the 3-by-3 submatrix for the *unlabeled* ABC TM in terms of the *labeled Hägg TMs*:

$$\begin{pmatrix} \mathcal{T}_{3i-2,3j-2} & \mathcal{T}_{3i-2,3j-1} & \mathcal{T}_{3i-2,3j} \\ \mathcal{T}_{3i-1,3j-2} & \mathcal{T}_{3i-1,3j-1} & \mathcal{T}_{3i-1,3j} \\ \mathcal{T}_{3i,3j-2} & \mathcal{T}_{3i,3j-1} & \mathcal{T}_{3i,3j} \end{pmatrix} = \begin{pmatrix} 0 & \mathsf{T}^{[1]}_{ij} & \mathsf{T}^{[0]}_{ij} \\ \mathsf{T}^{[0]}_{ij} & 0 & \mathsf{T}^{[1]}_{ij} \\ \mathsf{T}^{[1]}_{ij} & \mathsf{T}^{[0]}_{ij} & 0 \end{pmatrix}. \tag{7}$$

For nonmixing Hägg-machines, the above algorithm creates three disconnected ABC-machines, of which only one should be retained.

Furthermore, for mixing Hägg-machines, the probability from the stationary distribution over their states maps to a triplet of probabilities for the stationary distribution over the ABC-machine states:

$$\left\{p^{\mathrm{H}}_i\right\} \overset{\text{Hägg to } ABC}{\Longrightarrow} \left\{3p_{3i-2}, 3p_{3i-1}, 3p_{3i}\right\} \tag{8}$$

such that

[5] We use the same nomenclature to denote an SSC as previously used to denote a causal state cycle: the state sequence visited traversing the cycle is given in square brackets (Varn *et al.*, 2013*a*). For those cases where an ambiguity exists because the transition occurs on more than one symbol, we insert a subscript in parentheses denoting that symbol.

[6] Alternative constructions merely swap the labels of different states, but this choice of indexing affects the particular form of the TMs and how they are extracted from the Hägg-machine TMs. We choose the construction here for its intuitive and simple form.

$$\langle \boldsymbol{\pi}| = \left[p_1\ p_2\ p_3\ p_4\ \cdots\ p_{M_\mathrm{P}-1}\ p_{M_\mathrm{P}}\right] = \tfrac{1}{3}\left[p_1^\mathrm{H}\ p_1^\mathrm{H}\ p_1^\mathrm{H}\ p_2^\mathrm{H}\ \cdots\ p_{\mathsf{M}_\mathrm{H}}^\mathrm{H}\ p_{\mathsf{M}_\mathrm{H}}^\mathrm{H}\right]. \quad (9)$$

The reader should check that applying the rote expansion method given here results in the same HMM for the GM process as we found in §3.1.

4. Correlation functions from HMMs

In this section we derive expressions for the CFs in terms of the *ABC*-machine. We present two layers of analysis: one directly in terms of the TMs in §4.1, followed by one based on spectral analysis of the *ABC*-machine in §4.2. From the results of this latter method, we find the conditions under which the CFs decay to asymptotic values in §4.3 and, additionally, we discover constraints on the modes of decay of the CFs in §4.4.

We introduce the family of cyclic relation functions $\hat{\xi}(x) \in \{\hat{\mathrm{c}}(x), \hat{\mathrm{a}}(x), \hat{\mathrm{s}}(x)\}$, where, for example,

$$\hat{\mathrm{c}}(x) = \begin{cases} B & \text{if } x = A \\ C & \text{if } x = B \\ A & \text{if } x = C \end{cases}. \quad (10)$$

Thus, $\hat{\mathrm{c}}(x)$ is the cyclic permutation function. Complementarily, $\hat{\mathrm{a}}(x)$ performs anticyclic permutation among $x \in \{A, B, C\}$; $\hat{\mathrm{s}}(x)$ performs the identity operation among $x \in \{A, B, C\}$ and is suggestively denoted with an 's' for *same*. In terms of the absolute position of the MLs, *i.e.*, $\mathcal{A}_\mathrm{P} = \{A, B, C\}$, the CFs directly relate to the products of particular sequences of TMs. This perspective suggests a way to uncover the precise relation between the CFs and the TMs. Using this, we then give a closed-form expression for $Q_\xi(n)$ for any given HMM.

4.1. CFs from TMs

As a prelude to developing a general method to calculate any arbitrary CF from the *ABC*-machine, let us first consider the meaning of $Q_\mathrm{c}(3)$. In words, this is the probability that two MLs separated by two intervening MLs are cyclically related. Mathematically, we might start by writing this as

$$Q_\mathrm{c}(3) = \Pr(A**B) + \Pr(B**C) + \Pr(C**A), \quad (11)$$

where $*$ is a wildcard symbol denoting an indifference for the symbol observed in its place.[7] That is, $*$'s denote marginalizing over the intervening MLs such that, for example,

$$\Pr(A**B) = \sum_{x_1 \in \mathcal{A}_\mathrm{P}} \sum_{x_2 \in \mathcal{A}_\mathrm{P}} \Pr(Ax_1x_2B). \quad (12)$$

Making use of the TM formalism discussed previously, this becomes

$$\begin{aligned}
\Pr(A**B) &= \sum_{x_1 \in \mathcal{A}_\mathrm{P}} \sum_{x_2 \in \mathcal{A}_\mathrm{P}} \Pr(Ax_1x_2B) \\
&= \sum_{x_1 \in \mathcal{A}_\mathrm{P}} \sum_{x_2 \in \mathcal{A}_\mathrm{P}} \langle \boldsymbol{\pi}|\mathcal{T}^{[A]}\mathcal{T}^{[x_1]}\mathcal{T}^{[x_2]}\mathcal{T}^{[B]}|\mathbf{1}\rangle \\
&= \langle \boldsymbol{\pi}|\mathcal{T}^{[A]}\left(\sum_{x_1 \in \mathcal{A}_\mathrm{P}} \sum_{x_2 \in \mathcal{A}_\mathrm{P}} \mathcal{T}^{[x_1]}\mathcal{T}^{[x_2]}\right)\mathcal{T}^{[B]}|\mathbf{1}\rangle \\
&= \langle \boldsymbol{\pi}|\mathcal{T}^{[A]}\underbrace{\left(\sum_{x_1 \in \mathcal{A}_\mathrm{P}} \mathcal{T}^{[x_1]}\right)}_{=\mathcal{T}}\underbrace{\left(\sum_{x_2 \in \mathcal{A}_\mathrm{P}} \mathcal{T}^{[x_2]}\right)}_{=\mathcal{T}}\mathcal{T}^{[B]}|\mathbf{1}\rangle \\
&= \langle \boldsymbol{\pi}|\mathcal{T}^{[A]}(\mathcal{T})(\mathcal{T})\mathcal{T}^{[B]}|\mathbf{1}\rangle \\
&= \langle \boldsymbol{\pi}|\mathcal{T}^{[A]}\mathcal{T}^2\mathcal{T}^{[B]}|\mathbf{1}\rangle,
\end{aligned}$$

where $|\mathbf{1}\rangle$ is a column vector of 1's of length M_P. Hence, we can rewrite $Q_\mathrm{c}(3)$ as

$$\begin{aligned}
Q_\mathrm{c}(3) &= \Pr(A**B) + \Pr(B**C) + \Pr(C**A) \\
&= \langle \boldsymbol{\pi}|\mathcal{T}^{[A]}\mathcal{T}^2\mathcal{T}^{[B]}|\mathbf{1}\rangle + \langle \boldsymbol{\pi}|\mathcal{T}^{[B]}\mathcal{T}^2\mathcal{T}^{[C]}|\mathbf{1}\rangle \\
&\quad + \langle \boldsymbol{\pi}|\mathcal{T}^{[C]}\mathcal{T}^2\mathcal{T}^{[A]}|\mathbf{1}\rangle \\
&= \sum_{x \in \mathcal{A}_\mathrm{P}} \langle \boldsymbol{\pi}|\mathcal{T}^{[x]}\mathcal{T}^2\mathcal{T}^{[\hat{\mathrm{c}}(x)]}|\mathbf{1}\rangle.
\end{aligned}$$

For *mixing* *ABC*-machines, $\Pr(A**B) = \Pr(B**C) = \Pr(C**A) = \frac{1}{3}Q_\mathrm{c}(3)$, in which case the above reduces to

$$Q_\mathrm{c}(3) = 3\langle \boldsymbol{\pi}|\mathcal{T}^{[x_0]}\mathcal{T}^2\mathcal{T}^{[\hat{\mathrm{c}}(x_0)]}|\mathbf{1}\rangle, \quad \text{where } x_0 \in \mathcal{A}_\mathrm{P}.$$

The generalization to express any $Q_\xi(n)$ in terms of TMs may already be obvious by analogy. Nevertheless, we give a brief derivation for completeness, using similar concepts to those developed more explicitly above. For all $\xi \in \{\mathrm{c}, \mathrm{a}, \mathrm{s}\}$ and for all $n \in \{1, 2, 3, \ldots\}$, we can write the CFs as

$$\begin{aligned}
Q_\xi(n) &= \Pr(A\underbrace{*\cdots*}_{n-1*\mathrm{s}}\hat{\xi}(A)) + \Pr(B\underbrace{*\cdots*}_{n-1*\mathrm{s}}\hat{\xi}(B)) \\
&\quad + \Pr(C\underbrace{*\cdots*}_{n-1*\mathrm{s}}\hat{\xi}(C)) \\
&= \sum_{x_0 \in \mathcal{A}_\mathrm{P}} \Pr(x_0\underbrace{*\cdots*}_{n-1*\mathrm{s}}\hat{\xi}(x_0)) \\
&= \sum_{x_0 \in \mathcal{A}_\mathrm{P}} \sum_{w \in \mathcal{A}_\mathrm{P}^{n-1}} \Pr(x_0w\hat{\xi}(x_0)) \\
&= \sum_{x_0 \in \mathcal{A}_\mathrm{P}} \sum_{w \in \mathcal{A}_\mathrm{P}^{n-1}} \langle \boldsymbol{\pi}|\mathcal{T}^{[x_0]}\mathcal{T}^{[w]}\mathcal{T}^{[\hat{\xi}(x_0)]}|\mathbf{1}\rangle \\
&= \sum_{x_0 \in \mathcal{A}_\mathrm{P}} \langle \boldsymbol{\pi}|\mathcal{T}^{[x_0]}\left(\sum_{w \in \mathcal{A}_\mathrm{P}^{n-1}} \mathcal{T}^{[w]}\right)\mathcal{T}^{[\hat{\xi}(x_0)]}|\mathbf{1}\rangle \\
&= \sum_{x_0 \in \mathcal{A}_\mathrm{P}} \langle \boldsymbol{\pi}|\mathcal{T}^{[x_0]}\left(\prod_{i=1}^{n-1}\underbrace{\sum_{x_i \in \mathcal{A}_\mathrm{P}} \mathcal{T}^{[x_i]}}_{=\mathcal{T}}\right)\mathcal{T}^{[\hat{\xi}(x_0)]}|\mathbf{1}\rangle \\
&= \sum_{x_0 \in \mathcal{A}_\mathrm{P}} \langle \boldsymbol{\pi}|\mathcal{T}^{[x_0]}\mathcal{T}^{n-1}\mathcal{T}^{[\hat{\xi}(x_0)]}|\mathbf{1}\rangle, \quad (13)
\end{aligned}$$

where the stationary distribution $\langle \boldsymbol{\pi}|$ over states of the *ABC*-machine is found from equation (1). *The most general*

[7] While it is tempting to add the stipulation that no two consecutive symbols can be the same, this will fall out naturally from $Q_\mathrm{s}(1) = 0$ *via* the transition constraints built into the *ABC*-machine construction.

connection between CFs and TMs is given by equation (13) and this represents one of the main results of this paper.

As before, we might assume on physical grounds that

$$\Pr(A \underbrace{*\cdots*}_{n-1*\mathrm{s}} \hat{\xi}(A)) = \Pr(B \underbrace{*\cdots*}_{n-1*\mathrm{s}} \hat{\xi}(B)) = \Pr(C \underbrace{*\cdots*}_{n-1*\mathrm{s}} \hat{\xi}(C)). \tag{14}$$

For example, equation (14) is always true of mixing *ABC*-machines. This special case yields the more constrained set of equations:

$$Q_\xi(n) = 3\langle \boldsymbol{\pi} | \mathcal{T}^{[x_0]} \mathcal{T}^{n-1} \mathcal{T}^{[\hat{\xi}(x_0)]} | \mathbf{1} \rangle, \tag{15}$$

where $x_0 \in \mathcal{A}_\mathrm{P}$.

4.2. CFs from spectral decomposition

Although equation (13) is itself an important result, we can also apply a spectral decomposition of powers of the TM to provide a closed form that is even more useful and insightful. Ameliorating the computational burden, this result reduces the matrix powers in the above expressions to expressions involving only powers of scalars. Also, yielding theoretical insight, the closed forms reveal what types of behaviors can ever be expected of the CFs from stacking processes described by finite HMMs.

The most familiar case occurs when the TM is diagonalizable. Then, $\mathcal{T}^{n-1}$ can be found *via* diagonalizing the TM, making use of the fact that $\mathcal{T}^L = CD^LC^{-1}$, given the eigendecomposition $\mathcal{T} = CDC^{-1}$, where D is the diagonal matrix of eigenvalues. However, to understand the CF behavior, it is more appropriate to decompose the matrix in terms of its projection operators.

Moreover, an analytic expression for $\mathcal{T}^{n-1}$ can be found in terms of the projection operators even when the TM is not diagonalizable. Details are given elsewhere (Crutchfield *et al.*, 2013; Riechers & Crutchfield, 2015). By way of summarizing, though, in the general case the L-th iteration of the TM follows from

$$\mathcal{T}^L = \mathcal{Z}^{-1}\{(\mathbb{I} - z^{-1}\mathcal{T})^{-1}\}, \tag{16}$$

where $\mathbb{I}$ is the $M_\mathrm{P} \times M_\mathrm{P}$ identity matrix, $z \in \mathbb{C}$ is a continuous complex variable and $\mathcal{Z}^{-1}\{\cdot\}$ denotes the inverse z-transform (Oppenheim & Schafer, 1975) defined to operate elementwise:

$$\mathcal{Z}^{-1}(g(z)) \equiv \frac{1}{2\pi i} \oint_C z^{L-1} g(z)\, \mathrm{d}z \tag{17}$$

for the z-dependent matrix element $g(z)$ of $(\mathbb{I} - z^{-1}\mathcal{T})^{-1}$. Here, $\oint_C$ indicates a counterclockwise contour integration in the complex plane enclosing the entire unit circle.

For non-negative integers L, and with the allowance that $0^L = \delta_{L,0}$ for the case that $0 \in \Lambda_\mathcal{T}$, equation (16) becomes

$$\mathcal{T}^L = \sum_{\lambda \in \Lambda_\mathcal{T}} \sum_{m=0}^{\nu_\lambda - 1} \lambda^{L-m} \binom{L}{m} \mathcal{T}_\lambda (\mathcal{T} - \lambda\mathbb{I})^m, \tag{18}$$

where $\Lambda_\mathcal{T} = \{\lambda \in \mathbb{C} : \det(\lambda\mathbb{I} - \mathcal{T}) = 0\}$ is the set of $\mathcal{T}$'s eigenvalues, $\mathcal{T}_\lambda$ is the projection operator associated with the eigenvalue λ given by the elementwise residue of the resolvent $(z\mathbb{I} - \mathcal{T})^{-1}$ at $z \to \lambda$, the index ν_λ of the eigenvalue λ is the size of the largest Jordan block associated with λ, and

$$\binom{L}{m} = \frac{L!}{m!(L-m)!}$$

is the binomial coefficient. [Recall, *e.g.*, that $\binom{L}{0} = 1$, $\binom{L}{1} = L$, $\binom{L}{2} = \frac{1}{2!}L(L-1)$ and $\binom{L}{L} = 1$.] In terms of elementwise contour integration, we have

$$\mathcal{T}_\lambda = \frac{1}{2\pi i} \oint_{C_\lambda} (z\mathbb{I} - \mathcal{T})^{-1}\, \mathrm{d}z, \tag{19}$$

where C_λ is any contour in the complex plane enclosing the point $z_0 = \lambda$ – which may or may not be a singularity depending on the particular element of the resolvent matrix – but encloses no other singularities.

As guaranteed by the Perron–Frobenius theorem, all eigenvalues of the stochastic TM $\mathcal{T}$ lie on or within the unit circle. Moreover, the eigenvalues on the unit circle are guaranteed to have index one. The indices of all other eigenvalues must be less than or equal to one more than the difference between their algebraic a_λ and geometric g_λ multiplicities. Specifically:

$$\nu_\lambda - 1 \leq a_\lambda - g_\lambda \leq a_\lambda - 1 \quad \text{and} \quad a_\lambda = g_\lambda \quad \text{if } |\lambda| = 1.$$

Using equation (18) together with equation (13), the CFs can now be expressed as

$$Q_\xi(n) = \sum_{\lambda \in \Lambda_\mathcal{T}} \sum_{m=0}^{\nu_\lambda - 1} \left\langle \mathcal{T}^{\xi(\mathcal{A})}_{\lambda,m} \right\rangle \binom{n-1}{m} \lambda^{n-m-1}, \tag{20}$$

where $\langle \mathcal{T}^{\xi(\mathcal{A})}_{\lambda,m} \rangle$ is a complex-valued scalar:[8]

$$\left\langle \mathcal{T}^{\xi(\mathcal{A})}_{\lambda,m} \right\rangle \equiv \sum_{x_0 \in \mathcal{A}_\mathrm{P}} \langle \boldsymbol{\pi} | \mathcal{T}^{[x_0]} \mathcal{T}_\lambda (\mathcal{T} - \lambda\mathbb{I})^m \mathcal{T}^{[\hat{\xi}(x_o)]} | \mathbf{1} \rangle. \tag{21}$$

Evidently, the CFs' mathematical form [equation (20)] is strongly constrained for any stacking process that can be described by a finite HMM. Besides the expression's elegance, we note that its constrained form is very useful for the so-called 'inverse problem' of discovering the stacking process from CFs (Varn *et al.*, 2002, 2007, 2013*a*,*b*).

When $\mathcal{T}$ is diagonalizable, $\nu_\lambda = 1$ for all λ so that equation (18) simply reduces to

$$\mathcal{T}^L = \sum_{\lambda \in \Lambda_\mathcal{T}} \lambda^L \mathcal{T}_\lambda, \tag{22}$$

where the projection operators can be obtained more simply as

$$\mathcal{T}_\lambda = \prod_{\substack{\zeta \in \Lambda_\mathcal{T} \\ \zeta \neq \lambda}} \frac{\mathcal{T} - \zeta\mathbb{I}}{\lambda - \zeta}. \tag{23}$$

In the diagonalizable case, equation (20) reduces to

[8] $\langle \mathcal{T}^{\xi(\mathcal{A})}_{\lambda,m} \rangle$ is constant with respect to the relative layer displacement n. However, $\{\langle \mathcal{T}^{\xi(\mathcal{A})}_{\lambda,m} \rangle\}$ can be a function of a process's parameters.

$$Q_\xi(n) = \sum_{\lambda\in\Lambda_\mathcal{T}} \lambda^{n-1} \sum_{x_0\in\mathcal{A}_\mathrm{P}} \langle \boldsymbol{\pi}|\mathcal{T}^{[x_0]}\mathcal{T}_\lambda \mathcal{T}^{[\hat{\xi}(x_0)]}|\mathbf{1}\rangle$$
$$= \sum_{\lambda\in\Lambda_\mathcal{T}} \left\langle \mathcal{T}_\lambda^{\xi(\mathcal{A})} \right\rangle \lambda^{n-1}, \qquad (24)$$

where $\langle \mathcal{T}_\lambda^{\xi(\mathcal{A})}\rangle \equiv \langle \mathcal{T}_{\lambda,0}^{\xi(\mathcal{A})}\rangle$ is again a constant with respect to n:

$$\left\langle \mathcal{T}_\lambda^{\xi(\mathcal{A})} \right\rangle = \sum_{x_0\in\mathcal{A}_\mathrm{P}} \langle \boldsymbol{\pi}|\mathcal{T}^{[x_0]}\mathcal{T}_\lambda \mathcal{T}^{[\hat{\xi}(x_0)]}|\mathbf{1}\rangle. \qquad (25)$$

4.3. Asymptotic behavior of the CFs

From the spectral decomposition, it is apparent that the CFs converge to some constant value as $n\to\infty$, unless $\mathcal{T}$ has eigenvalues on the unit circle besides unity itself. If unity is the sole eigenvalue with a magnitude of one, then all other eigenvalues have magnitude less than unity and their contributions decay to negligibility for large enough n. Explicitly, if $\arg\max_{\lambda\in\Lambda_\mathcal{T}} |\lambda| = \{1\}$, then

$$\lim_{n\to\infty} Q_\xi(n) = \lim_{n\to\infty} \sum_{\lambda\in\Lambda_\mathcal{T}} \sum_{m=0}^{\nu_\lambda-1} \left\langle \mathcal{T}_{\lambda,m}^{\xi(\mathcal{A})} \right\rangle \binom{n-1}{m} \lambda^{n-m-1}$$
$$= \left\langle \mathcal{T}_1^{\xi(\mathcal{A})} \right\rangle$$
$$= \sum_{x_0\in\mathcal{A}_\mathrm{P}} \langle \boldsymbol{\pi}|\mathcal{T}^{[x_0]}\mathcal{T}_1 \mathcal{T}^{[\hat{\xi}(x_0)]}|\mathbf{1}\rangle$$
$$= \sum_{x_0\in\mathcal{A}_\mathrm{P}} \langle \boldsymbol{\pi}|\mathcal{T}^{[x_0]}|\mathbf{1}\rangle \langle \boldsymbol{\pi}|\mathcal{T}^{[\hat{\xi}(x_0)]}|\mathbf{1}\rangle$$
$$= \sum_{x_0\in\mathcal{A}_\mathrm{P}} \Pr(x_0)\Pr(\hat{\xi}(x_0)).$$

In the above, we used the fact that $\nu_1 = 1$ and that, for an ergodic process, $\mathcal{T}_1 = |\mathbf{1}\rangle\langle\boldsymbol{\pi}|$.

For mixing ABC-machines, $\Pr(x) = 1/3$ for all $x\in\mathcal{A}_\mathrm{P}$. That this is so should be evident from the graphical expansion method of §3.1. Therefore, mixing processes with $\arg\max_{\lambda\in\Lambda_\mathcal{T}} |\lambda| = \{1\}$ have CFs that all converge to 1/3:

$$\lim_{n\to\infty} Q_\xi(n) = \sum_{x_0\in\mathcal{A}_\mathrm{P}} \Pr(x_0)\Pr(\hat{\xi}(x_0))$$
$$= 3\left(\tfrac{1}{3}\times\tfrac{1}{3}\right)$$
$$= \tfrac{1}{3}.$$

Nonmixing processes with $\arg\max_{\lambda\in\Lambda_\mathcal{T}} |\lambda| = \{1\}$ can have their CFs converging to constants other than 1/3, depending on $\{\Pr(x) : x\in\mathcal{A}_\mathrm{P}\}$, although they are still constrained by $\sum_\xi Q_\xi(n) = 1$.

If other eigenvalues in $\Lambda_\mathcal{T}$ beside unity exist on the unit circle, then the CFs approach a periodic sequence as n gets large.

4.4. Modes of decay

Since $\mathcal{T}$ has no more eigenvalues than its dimension (*i.e.*, $|\Lambda_\mathcal{T}| \leq M_\mathrm{P}$), *equation* (20) *implies that the number of states in the ABC-machine for a stacking process puts an upper bound on the number of modes of decay*. Indeed, since unity is associated with stationarity, the number of modes of decay is strictly less than M_P. It is important to note that these modes do not always decay strictly exponentially: they are in general the product of a decaying exponential with a polynomial in n, and the CFs are sums of these products.

Even if – due to diagonalizability of $\mathcal{T}$ – there were only strictly exponentially decaying modes, it is simple but important to understand that there is generally more than one mode of exponential decay present in the CFs. And so, ventures to find *the* decay constant of a process are misleading unless it is explicitly acknowledged that one seeks, *e.g.*, the slowest decay mode. Even then, however, there are cases when the slowest decay mode only acts on a component of the CFs with negligible magnitude. In an extreme case, the slowest decay mode may not even be a large contributor to the CFs before the whole pattern is numerically indistinguishable from the asymptotic value.

In analyzing a broad range of CFs, nevertheless, many authors have been led to consider *correlation lengths*, also known as *characteristic lengths* (Tiwary & Pandey, 2007; Varn *et al.*, 2013*b*). The form of equation (20) suggests that this perspective will often be a clumsy oversimplification for understanding CFs. Regardless, if one wishes to assign a correlation length associated with an index-one mode of CF decay, we observe that the reciprocal of the correlation length is essentially the negative logarithm of the magnitude of the eigenvalue for that mode. We find that the typically reported correlation length ℓ_C derives from the second-largest contributing magnitude among the eigenvalues:

$$\ell_\mathrm{C}^{-1} = -\log|\zeta|, \quad \text{for } \zeta\in\arg\max_{\lambda\in\boldsymbol{\rho}} |\lambda|, \qquad (26)$$

where $\boldsymbol{\rho} = \{\lambda\in\Lambda_\mathcal{T}\setminus\{1\} : \langle \mathcal{T}_\lambda^{\xi(\mathcal{A})}\rangle \neq 0\}$.

Guided by equation (20), we suggest that a true understanding of CF behavior involves finding $\Lambda_\mathcal{T}$ with the corresponding eigenvalue indices and the amplitude of each mode's contribution $\{\langle \mathcal{T}_{\lambda,m}^{\xi(\mathcal{A})}\rangle\}$.

This now completes our theoretical development, and in the next section we apply these techniques to three examples.

5. Examples

5.1. *C* polytypes and random ML stacking: IID processes

Although real materials often display much more complex behaviors, as a pedagogical exercise the random stacking of MLs in CPSs has often been treated (Guinier, 1963) to study stacking faults. This stacking process is the simplest stacking arrangement that can be imagined,[9] and there are previous analytical results that can be compared to the techniques developed here. In statistics parlance, this process is an *Independent and Identically Distributed* (IID) process (Cover & Thomas, 2006).

[9] This is not mere hyperbole. It is possible to quantify a process's structural organization in the form of its *statistical complexity* C_μ, which measures the internal information processing required to produce the pattern (Crutchfield & Young, 1989; Crutchfield, 2012; Varn *et al.*, 2013*a*). In the present case $C_\mu = 0$ bits, the minimum value.

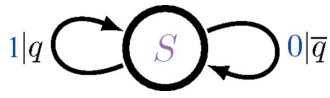

Figure 3
Hägg-machine for the IID process. When $q = 1$, the IID process generates a string of 1's, which is physically the $3C^+$ stacking structure. Conversely, when $q = 0$, the structure corresponds to the $3C^-$ structure. For $q = 1/2$, the MLs are stacked as randomly as possible. Here and elsewhere we adopt the convention that a bar over a variable means one minus that variable, *i.e.* $\overline{q} \equiv 1 - q$, with $q \in [0, 1]$.

Let us assume that the placement of MLs is independent of the previous MLs scanned, except that it of course must obey the stacking constraints. The Hägg-machine that describes this process is shown in Fig. 3. We allow for the possibility that there might be a bias in the stacking order, and we assign a probability q that the next layer is cyclically related to its predecessor. Thus, the 1-by-1 symbol-labeled TMs for the Hägg-machine are

$$\mathsf{T}^{[1]} = [q] \quad \text{and} \quad \mathsf{T}^{[0]} = [\overline{q}],$$

where $\overline{q} \equiv 1 - q$, with $q \in [0, 1]$.

The physical interpretation of the IID process is straightforward. In the case where $q = 1$, the process generates a stacking sequence of all 1's, giving a physical stacking structure of $\ldots ABCABCABC \ldots$. We recognize this as the $3C^+$ crystal structure. Similarly, for $q = 0$, the process generates a stacking sequence of all 0's, which is the $3C^-$ crystal structure. For those cases where q is near but not quite at its extreme values, the stacking structure is $3C$ with randomly distributed deformation faults. When $q = \frac{1}{2}$, the MLs are stacked in a completely random fashion.

Now, we must determine whether this is a mixing or nonmixing Hägg-machine. We note that there are two SSCs, namely $[\mathsf{S}_{(0)}]$ and $[\mathsf{S}_{(1)}]$. The winding numbers for each are $W^{[\mathsf{S}_{(1)}]} = 1$ and $W^{[\mathsf{S}_{(0)}]} = -1$, yielding $W^{[\mathsf{S}_{(1)}]} \pmod 3 = 1$ and $W^{[\mathsf{S}_{(0)}]} \pmod 3 = 2$. Since at least one of these is not equal to zero, the Hägg-machine is mixing, and we need to expand the Hägg-machine into the ABC-machine. This is shown in Fig. 4.

The ABC-machine TMs can either be directly written down from inspecting Fig. 4 or by using the rote expansion algorithm of §3.3, using equations (2) and (3). By either method we find the 3-by-3 TMs to be

$$\mathcal{T}^{[A]} = \begin{bmatrix} 0 & 0 & 0 \\ \overline{q} & 0 & 0 \\ q & 0 & 0 \end{bmatrix}, \quad \mathcal{T}^{[B]} = \begin{bmatrix} 0 & q & 0 \\ 0 & 0 & 0 \\ 0 & \overline{q} & 0 \end{bmatrix}$$

and

$$\mathcal{T}^{[C]} = \begin{bmatrix} 0 & 0 & \overline{q} \\ 0 & 0 & q \\ 0 & 0 & 0 \end{bmatrix}.$$

The internal-state TM then is their sum:

$$\mathcal{T} = \begin{bmatrix} 0 & q & \overline{q} \\ \overline{q} & 0 & q \\ q & \overline{q} & 0 \end{bmatrix}.$$

The eigenvalues of the ABC TM are

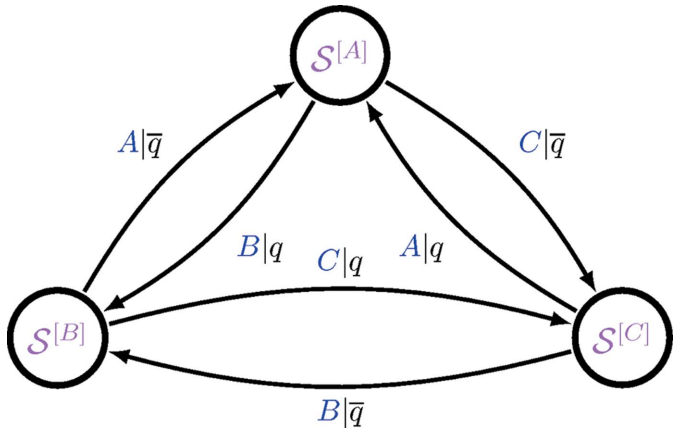

Figure 4
ABC-machine for the IID process. The single state of the Hägg-machine has expanded into three.

$$\Lambda_{\mathcal{T}} = \{1, \Omega, \Omega^*\},$$

where

$$\Omega \equiv -\frac{1}{2} + i\frac{3^{1/2}}{2}(4q^2 - 4q + 1)^{1/2}$$

and Ω^* is its complex conjugate. Already, *via* equation (26), we can identify what the characteristic length of the CFs will be. In particular, $\ell_{\mathrm{C}}^{-1} = -\log|\Omega| = -\frac{1}{2}\log(1 - 3q + 3q^2)$ yields

$$\ell_{\mathrm{C}} = -\frac{2}{\log(1 - 3q + 3q^2)}.$$

If we identify q with the deformation faulting parameter α in the model introduced by Estevez-Rams *et al.* (2008) (see the next example in §5.2, the RGDF process), this is identical to the result obtained there in equation (35). There is much more structural information in the CFs, however, than a single characteristic length would suggest. This fact will become especially apparent as our examples become more sophisticated.

According to equation (13), we can obtain the CFs *via*

$$Q_{\xi}(n) = \sum_{x_0 \in \mathcal{A}_{\mathrm{P}}} \langle \boldsymbol{\pi} | \mathcal{T}^{[x_0]} \mathcal{T}^{n-1} \mathcal{T}^{[\hat{\xi}(x_0)]} | \mathbf{1} \rangle.$$

The stationary distribution over the ABC-machine states is found from equation (1):

$$\langle \boldsymbol{\pi} | = \left[\tfrac{1}{3}\ \tfrac{1}{3}\ \tfrac{1}{3}\right].$$

Furthermore, an analytic expression for $\mathcal{T}^{n-1}$ follows from the z-transform as given in equation (16). As a start, we find

$$\mathbb{I} - z^{-1}\mathcal{T} = \begin{bmatrix} 1 & -q/z & -\overline{q}/z \\ -\overline{q}/z & 1 & -q/z \\ -q/z & -\overline{q}/z & 1 \end{bmatrix}$$

and its inverse

$$(\mathbb{I}-z^{-1}\mathcal{T}) = \frac{1}{(1-z^{-1})(1-\Omega z^{-1})(1-\Omega^* z^{-1})} \times \begin{bmatrix} 1-q\overline{q}z^{-2} & qz^{-1}+\overline{q}^2z^{-2} & \overline{q}z^{-1}+q^2z^{-2} \\ \overline{q}z^{-1}+q^2z^{-2} & 1-q\overline{q}z^{-2} & qz^{-1}+\overline{q}^2z^{-2} \\ qz^{-1}+\overline{q}^2z^{-2} & \overline{q}z^{-1}+q^2z^{-2} & 1-q\overline{q}z^{-2} \end{bmatrix}.$$

Upon partial fraction expansion, we obtain

$$\begin{aligned}(\mathbb{I}-z^{-1}\mathcal{T})^{-1} &= \frac{1}{3}\frac{1}{(1-z^{-1})}\begin{bmatrix}1&1&1\\1&1&1\\1&1&1\end{bmatrix} \\ &+ \frac{1}{(\Omega-1)(\Omega-\Omega^*)}\frac{1}{(1-\Omega z^{-1})}\begin{bmatrix}\Omega^2-q\overline{q} & q\Omega+\overline{q}^2 & \overline{q}\Omega+q^2\\ \overline{q}\Omega+q^2 & \Omega^2-q\overline{q} & q\Omega+\overline{q}^2\\ q\Omega+\overline{q}^2 & \overline{q}\Omega+q^2 & \Omega^2-q\overline{q}\end{bmatrix} \\ &+ \frac{1}{(\Omega^*-1)(\Omega^*-\Omega)}\frac{1}{(1-\Omega^* z^{-1})}\begin{bmatrix}\Omega^{*2}-q\overline{q} & q\Omega^*+\overline{q}^2 & \overline{q}\Omega^*+q^2\\ \overline{q}\Omega^*+q^2 & \Omega^{*2}-q\overline{q} & q\Omega^*+\overline{q}^2\\ q\Omega^*+\overline{q}^2 & \overline{q}\Omega^*+q^2 & \Omega^{*2}-q\overline{q}\end{bmatrix},\end{aligned} \tag{27}$$

for $q \neq 1/2$. (The special case of $q = 1/2$ is discussed in the next subsection.) Finally, we take the inverse z-transform of equation (27) to obtain an expression for the L-th iterate of the TM:

$$\begin{aligned}\mathcal{T}^L &= \mathcal{Z}^{-1}\left\{(\mathbb{I}-z^{-1}\mathcal{T})^{-1}\right\} \\ &= \frac{1}{3}\begin{bmatrix}1&1&1\\1&1&1\\1&1&1\end{bmatrix} \\ &+ \frac{\Omega^L}{(\Omega-1)(\Omega-\Omega^*)}\begin{bmatrix}\Omega^2-q\overline{q} & q\Omega+\overline{q}^2 & \overline{q}\Omega+q^2\\ \overline{q}\Omega+q^2 & \Omega^2-q\overline{q} & q\Omega+\overline{q}^2\\ q\Omega+\overline{q}^2 & \overline{q}\Omega+q^2 & \Omega^2-q\overline{q}\end{bmatrix} \\ &+ \frac{\Omega^{*L}}{(\Omega^*-1)(\Omega^*-\Omega)}\begin{bmatrix}\Omega^{*2}-q\overline{q} & q\Omega^*+\overline{q}^2 & \overline{q}\Omega^*+q^2\\ \overline{q}\Omega^*+q^2 & \Omega^{*2}-q\overline{q} & q\Omega^*+\overline{q}^2\\ q\Omega^*+\overline{q}^2 & \overline{q}\Omega^*+q^2 & \Omega^{*2}-q\overline{q}\end{bmatrix}.\end{aligned}$$

These pieces are all we need to calculate the CFs. Let's start with $Q_s(n)$. First, we find

$$\langle\boldsymbol{\pi}|\mathcal{T}^{[A]} = \begin{bmatrix}\frac{1}{3} & 0 & 0\end{bmatrix}$$

and

$$\mathcal{T}^{[\hat{\mathfrak{s}}(A)]}|\mathbf{1}\rangle = \mathcal{T}^{[A]}|\mathbf{1}\rangle = \begin{bmatrix}0\\ \overline{q}\\ q\end{bmatrix}.$$

Then

$$\begin{aligned}\langle\boldsymbol{\pi}|\mathcal{T}^{[A]}\mathcal{T}^{n-1} &= \frac{1}{9}[1\ 1\ 1] \\ &+ \frac{1}{3}\frac{\Omega^{n-1}}{(\Omega-1)(\Omega-\Omega^*)}\begin{bmatrix}\Omega^2-q\overline{q} & q\Omega+\overline{q}^2 & \overline{q}\Omega+q^2\end{bmatrix} \\ &+ \frac{1}{3}\frac{\Omega^{*n-1}}{(\Omega^*-1)(\Omega^*-\Omega)}\begin{bmatrix}\Omega^{*2}-q\overline{q} & q\Omega^*+\overline{q}^2 & \overline{q}\Omega^*+q^2\end{bmatrix}\end{aligned} \tag{28}$$

and

$$\begin{aligned}\langle\boldsymbol{\pi}|\mathcal{T}^{[A]}\mathcal{T}^{n-1}\mathcal{T}^{[A]}|\mathbf{1}\rangle &= \frac{1}{9} + \frac{1}{3}\frac{\Omega^{n-1}}{(\Omega-1)(\Omega-\Omega^*)}(2q\overline{q}\Omega+\Omega\Omega^*) \\ &+ \frac{1}{3}\frac{\Omega^{*n-1}}{(\Omega^*-1)(\Omega^*-\Omega)}(2q\overline{q}\Omega^*+\Omega\Omega^*).\end{aligned} \tag{29}$$

One can verify that equation (15) can be applied in lieu of equation (13), which saves some effort in finding the final result, which is

$$Q_s(n) = \frac{1}{3} + 2\mathrm{Re}\left\{\frac{\Omega^n}{(\Omega-1)(\Omega-\Omega^*)}(2q\overline{q}+\Omega^*)\right\}. \tag{30}$$

The cyclic and anticyclic CFs can also be calculated from equation (15) using the result we have already obtained in equation (28). A quick calculation yields

$$\mathcal{T}^{[\hat{\mathfrak{c}}(A)]}|\mathbf{1}\rangle = \mathcal{T}^{[B]}|\mathbf{1}\rangle = \begin{bmatrix}q\\0\\\overline{q}\end{bmatrix}$$

and

$$\mathcal{T}^{[\hat{\mathfrak{a}}(A)]}|\mathbf{1}\rangle = \mathcal{T}^{[C]}|\mathbf{1}\rangle = \begin{bmatrix}\overline{q}\\q\\0\end{bmatrix}.$$

Then, we have

$$\begin{aligned}Q_c(n) &= 3\langle\boldsymbol{\pi}|\mathcal{T}^{[A]}\mathcal{T}^{n-1}\mathcal{T}^{[B]}|\mathbf{1}\rangle \\ &= \frac{1}{3} + 2\mathrm{Re}\left\{\frac{\Omega^n}{(\Omega-1)(\Omega-\Omega^*)}(\overline{q}^2+q\Omega)\right\}\end{aligned} \tag{31}$$

and

$$\begin{aligned}Q_a(n) &= 3\langle\boldsymbol{\pi}|\mathcal{T}^{[A]}\mathcal{T}^{n-1}\mathcal{T}^{[C]}|\mathbf{1}\rangle \\ &= \frac{1}{3} + 2\mathrm{Re}\left\{\frac{\Omega^n}{(\Omega-1)(\Omega-\Omega^*)}(q^2+\overline{q}\Omega)\right\}.\end{aligned} \tag{32}$$

All of this subsection's results hold for the whole range of $q \in [0, \frac{1}{2}) \cup (\frac{1}{2}, 1]$, where all $\mathcal{T}$'s eigenvalues are distinct. However, for $q = 1/2$, the two complex conjugate eigenvalues, Ω and Ω^*, lose their imaginary components, becoming repeated eigenvalues. This requires special treatment.[10] We address the case of $q = 1/2$ in the next subsection, which is of interest in its own right as being the most random possible stacking sequence allowed.

5.1.1. A fair coin? For a completely random stacking of MLs, such that $q = 1/2$, the relative orientations of the MLs are effectively assigned by a fair coin. The resulting TM is symmetric with repeated eigenvalues, implying that, superficially at least, the CFs take on a special form.[11]

To obtain the CFs for the Fair Coin IID process, we follow the procedure of the previous subsection with all of the same

[10] Indeed, the straightforward z-transform approach yielding the CF equations given in this section appears to need special treatment for $q = 1/2$. However, a more direct spectral perspective as developed in §4.2 shows that since $\mathcal{T}$ is diagonalizable for all q, all eigenvalues have index of one and so yield CFs of the simple form of equation (24).

[11] But since the TM remains diagonalizable, the CFs retain the simple form of equation (24).

results through equation (27) which, with $q = 1/2$ and $\Omega|_{q=1/2} = \Omega^*|_{q=1/2} = -1/2$, can now be written as

$$(\mathbb{I} - z^{-1}\mathcal{T})^{-1} = \frac{1}{(1 - z^{-1})(1 + \frac{1}{2}z^{-1})^2} \times \begin{bmatrix} 1 - \frac{1}{4}z^{-2} & \frac{1}{2}z^{-1} + \frac{1}{4}z^{-2} & \frac{1}{2}z^{-1} + \frac{1}{4}z^{-2} \\ \frac{1}{2}z^{-1} + \frac{1}{4}z^{-2} & 1 - \frac{1}{4}z^{-2} & \frac{1}{2}z^{-1} + \frac{1}{4}z^{-2} \\ \frac{1}{2}z^{-1} + \frac{1}{4}z^{-2} & \frac{1}{2}z^{-1} + \frac{1}{4}z^{-2} & 1 - \frac{1}{4}z^{-2} \end{bmatrix}.$$

However, the repeated factor in the denominator yields a new partial fraction expansion. Applying the inverse z-transform gives the L-th iterate of the TM[12] as

$$\mathcal{T}^L = \mathcal{Z}^{-1}\left\{\left(\mathbb{I} - z^{-1}\mathcal{T}\right)^{-1}\right\} = \frac{1}{3}\begin{bmatrix} 1 & 1 & 1 \\ 1 & 1 & 1 \\ 1 & 1 & 1 \end{bmatrix} + \frac{1}{3}\left(-\frac{1}{2}\right)^L \begin{bmatrix} 2 & -1 & -1 \\ -1 & 2 & -1 \\ -1 & -1 & 2 \end{bmatrix}.$$

Then, we find

$$\langle \boldsymbol{\pi}|\mathcal{T}^{[A]}\mathcal{T}^{n-1} = \frac{1}{9}[1\ 1\ 1] + \frac{1}{9}\left(-\frac{1}{2}\right)^{n-1}[2\ -1\ -1],$$

with the final result that

$$Q_s(n) = 3\langle \boldsymbol{\pi}|\mathcal{T}^{[A]}\mathcal{T}^{n-1}\mathcal{T}^{[A]}|\mathbf{1}\rangle = \frac{1}{3} + \frac{2}{3}\left(-\frac{1}{2}\right)^n, \quad (33)$$

$$Q_c(n) = 3\langle \boldsymbol{\pi}|\mathcal{T}^{[A]}\mathcal{T}^{n-1}\mathcal{T}^{[B]}|\mathbf{1}\rangle = \frac{1}{3} - \frac{1}{3}\left(-\frac{1}{2}\right)^n \quad (34)$$

and

$$Q_a(n) = 3\langle \boldsymbol{\pi}|\mathcal{T}^{[A]}\mathcal{T}^{n-1}\mathcal{T}^{[C]}|\mathbf{1}\rangle = \frac{1}{3} - \frac{1}{3}\left(-\frac{1}{2}\right)^n. \quad (35)$$

For $q = 1/2$, we see that $Q_c(n)$ and $Q_a(n)$ are identical, but this is not generally the case as one can check for other values of q in equations (31) and (32).

Fig. 5 shows a graph of the TM's eigenvalues in the complex plane as q is varied. Notice that there is an eigenvalue at 1 for all values of q. This is a generic feature, and we always find such an eigenvalue. The other two eigenvalues start at the other two cube roots of unity for $q \in \{0, 1\}$ and, as $q \to 1/2$, they migrate to the point $-1/2$ and become degenerate when $q = 1/2$. It is this degeneracy that requires the special treatment given in this section.

It is interesting that even the Fair Coin Hägg-machine produces structured CFs. This is because, even though the allowed transitions of the underlying ABC-machine are randomized, not all transitions are allowed. For example, if we start with an A ML, the next ML has a zero probability of being an A, a 1/2 probability of being a B, and a 1/2 probability of being a C. Then, the *next* ML has a rebounding 1/2 probability of being an A while the probability of being either a B or C is each only 1/4. So, we see that the underlying process has structure, and there is nothing we can do, given the physical constraints, to make the CFs completely random.

When we can compare our expressions for CFs at $q = 1/2$ to those derived previously by elementary means (Guinier, 1963; Varn, 2001), we find agreement. Note however that unlike in these earlier treatments, here there was no need to assume a recursion relationship.

Figs. 6 and 7 show $Q_s(n)$ *versus* n for the IID process with $q = 0.1$ and $q = 0.3$, respectively, as computed from equation

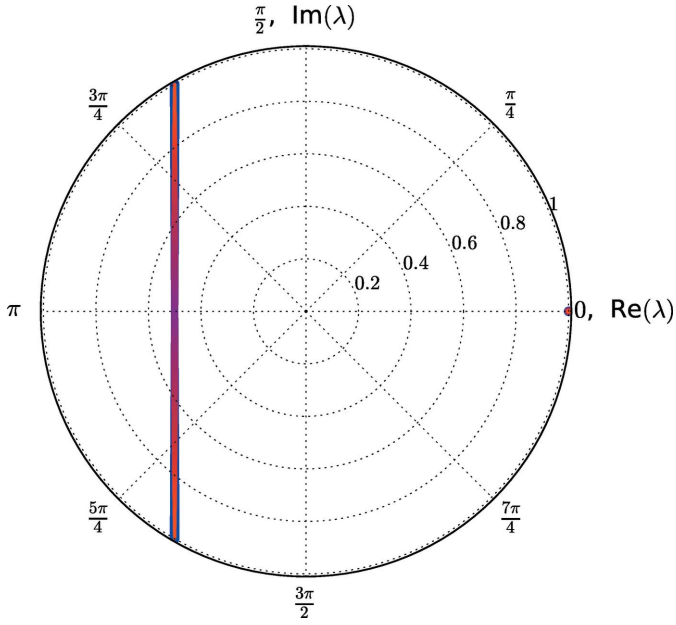

Figure 5
TM's eigenvalues in the complex plane for the IID process as q is varied. Note that there is always an eigenvalue at 1.

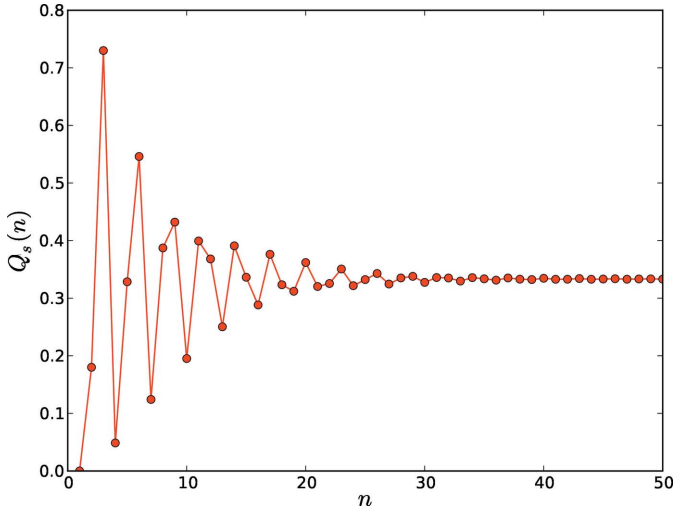

Figure 6
$Q_s(n)$ *versus* n for $q = 0.1$ the IID process.

[12] By inspection, we can verify that this decomposition still yields $\mathcal{T}^0$ as the identity matrix and $\mathcal{T}^1 = \mathcal{T}$, as must be the case. More interestingly, the decaying deviation from the asymptotic matrix is oscillatory.

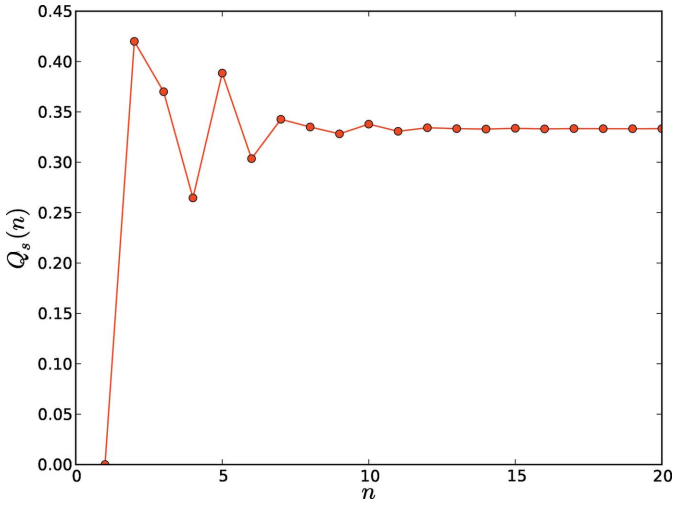

Figure 7
$Q_s(n)$ *versus* n for $q = 0.3$ the IID process.

(30). In each case the CFs decay to an asymptotic value of 1/3, although this decay is faster for $q = 0.3$. This is not surprising, as one interpretation for the IID process with $q = 0.1$ is that of a $3C^+$ crystal interspersed with 10% random deformation faults.

5.2. Random growth and deformation faults in layered 3*C* and 2*H* CPSs: the RGDF process

Estevez-Rams *et al.* (2008) recently showed that simultaneous random growth and deformation stacking faults (SFs) in 2*H* and 3*C* CPSs can be modeled for all values of the fault parameters by a simple HMM, and this is shown in Fig. 8. We refer to this process as the *Random Growth and Deformation Faults* (RGDF) process.[13] As has become convention (Warren, 1969; Estevez-Rams *et al.*, 2008), α refers to deformation faulting and β refers to growth faults.

The HMM describing the RGDF process is unlike any of the others considered here in that on emission of a symbol from a state, the successor state is *not* uniquely specified. For example, $\mathcal{U} \xrightarrow{0} \mathcal{U}$ and $\mathcal{U} \xrightarrow{0} \mathcal{V}$; *i.e.*, being in state $\mathcal{U}$ and emitting a 0 does not uniquely determine the next state. Such representations were previously called *nondeterministic* (Hopcroft & Ullman, 1979), but to avoid a conflict in terminology we prefer the term *nonunifilar* (Ephraim & Merhav, 2002; Ellison *et al.*, 2009). Since ε-machines are unifilar (Crutchfield & Young, 1989; Shalizi & Crutchfield, 2001), the HMM representing the RGDF process is not an ε-machine. Nonetheless, the techniques we have developed are applicable: CFs do not require unifilar HMMs for their calculations, as do other properties such as the entropy density.

Inspecting Fig. 8, the RGDF Hägg-machine's TMs are seen to be [equations (1) and (2) of Estevez-Rams *et al.*, 2008]

$$\mathsf{T}^{[0]} = \begin{bmatrix} \alpha\overline{\beta} & \overline{\alpha}\beta \\ \alpha\beta & \overline{\alpha}\overline{\beta} \end{bmatrix} \quad \text{and} \quad \mathsf{T}^{[1]} = \begin{bmatrix} \overline{\alpha}\overline{\beta} & \alpha\beta \\ \overline{\alpha}\beta & \alpha\overline{\beta} \end{bmatrix},$$

where $\alpha \in [0, 1]$ and $\overline{\alpha} \equiv 1 - \alpha$, such that $\alpha + \overline{\alpha} = 1$, and $\beta \in [0, 1]$ and $\overline{\beta} \equiv 1 - \beta$, such that $\beta + \overline{\beta} = 1$. There are eight SSCs and, if at least one of them has $W^{\mathrm{SSC}} \pmod 3 \neq 0$, the Hägg-machine is mixing. The self-state transitions each generate a nonvanishing $W^{\mathrm{SSC}} \pmod 3$, so for the Hägg-machine to be nonmixing, these transitions must be absent. Indeed, there are only two SSCs that have vanishing winding numbers, and these are $[\mathcal{U}_{(0)}\mathcal{V}_{(1)}]$ and $[\mathcal{U}_{(1)}\mathcal{V}_{(0)}]$. These, and only these, SSCs can exist if $\overline{\beta} = 0$ and $\alpha \in \{0, 1\}$. Thus, the Hägg-machine is nonmixing only for the parameter settings $\beta = 1$ and $\alpha \in \{0, 1\}$, which corresponds to the 2*H* crystal structure.

From the Hägg-machine, we obtain the corresponding TMs of the *ABC*-machine for $\alpha, \beta \in (0, 1)$ by the rote expansion method (§3.3):

$$\mathcal{T}^{[A]} = \begin{bmatrix} 0 & 0 & 0 & 0 & 0 & 0 \\ \alpha\overline{\beta} & 0 & 0 & \overline{\alpha}\beta & 0 & 0 \\ \overline{\alpha}\overline{\beta} & 0 & 0 & \alpha\beta & 0 & 0 \\ 0 & 0 & 0 & 0 & 0 & 0 \\ \alpha\beta & 0 & 0 & \overline{\alpha}\overline{\beta} & 0 & 0 \\ \overline{\alpha}\beta & 0 & 0 & \alpha\overline{\beta} & 0 & 0 \end{bmatrix},$$

$$\mathcal{T}^{[B]} = \begin{bmatrix} 0 & \overline{\alpha}\overline{\beta} & 0 & 0 & \alpha\beta & 0 \\ 0 & 0 & 0 & 0 & 0 & 0 \\ 0 & \alpha\overline{\beta} & 0 & 0 & \overline{\alpha}\beta & 0 \\ 0 & \overline{\alpha}\beta & 0 & 0 & \alpha\overline{\beta} & 0 \\ 0 & 0 & 0 & 0 & 0 & 0 \\ 0 & \alpha\beta & 0 & 0 & \overline{\alpha}\overline{\beta} & 0 \end{bmatrix}$$

and

$$\mathcal{T}^{[C]} = \begin{bmatrix} 0 & 0 & \alpha\overline{\beta} & 0 & 0 & \overline{\alpha}\beta \\ 0 & 0 & \overline{\alpha}\overline{\beta} & 0 & 0 & \alpha\beta \\ 0 & 0 & 0 & 0 & 0 & 0 \\ 0 & 0 & \alpha\beta & 0 & 0 & \overline{\alpha}\overline{\beta} \\ 0 & 0 & \overline{\alpha}\beta & 0 & 0 & \alpha\overline{\beta} \\ 0 & 0 & 0 & 0 & 0 & 0 \end{bmatrix},$$

and the orientation-agnostic state-to-state TM:

$$\mathcal{T} = \mathcal{T}^{[A]} + \mathcal{T}^{[B]} + \mathcal{T}^{[C]}.$$

Explicitly, we have:

$$\mathcal{T} = \begin{bmatrix} 0 & \overline{\alpha}\overline{\beta} & \alpha\overline{\beta} & 0 & \alpha\beta & \overline{\alpha}\beta \\ \alpha\overline{\beta} & 0 & \overline{\alpha}\overline{\beta} & \overline{\alpha}\beta & 0 & \alpha\beta \\ \overline{\alpha}\overline{\beta} & \alpha\overline{\beta} & 0 & \alpha\beta & \overline{\alpha}\beta & 0 \\ 0 & \overline{\alpha}\beta & \alpha\beta & 0 & \alpha\overline{\beta} & \overline{\alpha}\overline{\beta} \\ \alpha\beta & 0 & \overline{\alpha}\beta & \overline{\alpha}\overline{\beta} & 0 & \alpha\overline{\beta} \\ \overline{\alpha}\beta & \alpha\beta & 0 & \alpha\overline{\beta} & \overline{\alpha}\overline{\beta} & 0 \end{bmatrix}.$$

$\mathcal{T}$'s eigenvalues satisfy $\det(\mathcal{T} - \lambda\mathbb{I}) = 0$. Here, with $a \equiv \alpha\beta$, $b \equiv \alpha\overline{\beta}$, $c \equiv \overline{\alpha}\beta$ and $d \equiv \overline{\alpha}\overline{\beta}$, we have

[13] Estevez-Rams *et al.* (2008) give a thorough and detailed discussion of the RGDF process, and readers interested in a comprehensive motivation and derivation of the RGDF process are urged to consult that reference.

$$\det(\mathcal{T}-\lambda\mathbb{I}) = \left[(\lambda-(b+d))^2-(a+c)^2\right] \times \left[\lambda^2+\lambda(b+d)+ac-bd-a^2-c^2+b^2+d^2\right]^2 = 0,$$

from which we obtain the eigenvalues: $\lambda = b+d\pm(a+c)$ and $\lambda = \frac{1}{2}(b+d)\pm\frac{1}{2}\left[4(a+c)^2-3(b+d)^2+12(bd-ac)\right]^{\frac{1}{2}}$. To get back to α's and β's, we note that $a+c=\beta$, $b+d=\overline{\beta}$, $ac=\beta^2\alpha\overline{\alpha}$ and $bd=\overline{\beta}^2\alpha\overline{\alpha}$. It also follows that $b+d+a+c=1$, $b+d-(a+c)=\overline{\beta}-\beta=1-2\beta$ and $bd-ac=\alpha\overline{\alpha}(\overline{\beta}^2-\beta^2)=\alpha\overline{\alpha}(1-2\beta)=\alpha\overline{\alpha}(\overline{\beta}-\beta)$. Hence, after simplification, the set of $\mathcal{T}$'s eigenvalues can be written as

$$\Lambda_{\mathcal{T}} = \left\{1, 1-2\beta, -\tfrac{1}{2}(1-\beta)\pm\tfrac{1}{2}\sigma^{1/2}\right\}, \tag{36}$$

with

$$\sigma \equiv 4\beta^2-3\overline{\beta}^2+12\alpha\overline{\alpha}(\overline{\beta}-\beta) \tag{37}$$

$$= -3+12\alpha+6\beta-12\alpha^2 + \beta^2-24\alpha\beta+24\alpha^2\beta. \tag{38}$$

Except for measure-zero submanifolds along which the eigenvalues become extra degenerate, throughout the parameter range the eigenvalues' algebraic multiplicities are: $a_1=1$, $a_{1-2\beta}=1$, $a_{-\frac{1}{2}(1-\beta+\sigma^{1/2})}=2$ and $a_{-\frac{1}{2}(1-\beta-\sigma^{1/2})}=2$. Moreover, the *index* of all eigenvalues is 1 except along $\sigma=0$.

Immediately from the eigenvalues and their corresponding indices, we know all possible characteristic modes of CF decay. All that remains is to find the contributing amplitude of each characteristic mode. For comparison, note that our σ turns out to be equivalent to the all-important $-s^2$ term defined in equation (28) of Estevez-Rams *et al.* (2008).

Equations (36) and (37) reveal an obvious symmetry between α and $\overline{\alpha}$ that is *not* present between β and $\overline{\beta}$. In particular, $\mathcal{T}$'s eigenvalues are invariant under exchange of α and $\overline{\alpha}$ – the CFs will decay in the same manner for α values symmetric about 1/2. There is no such symmetry between β and $\overline{\beta}$. Parameter-space organization is seen nicely in panel (c) of Fig. 6 from Estevez-Rams *et al.* (2008). Importantly, in that figure $\sigma=0$ should be seen as the critical line organizing a phase transition in parameter space. Here, we will show that the $\sigma=0$ line actually corresponds to nondiagonalizability of the TM and, thus, to the qualitatively different polynomial behavior in the decay of the CFs predicted by our equation (20).

Note that since $\mathcal{T}$ is doubly stochastic (*i.e.*, all rows sum to one *and* all columns sum to one), the all-ones vector is not only the right eigenvector associated with the eigenvalue of unity, but also the left eigenvector associated with unity. Moreover, since the stationary distribution $\langle\boldsymbol{\pi}|$ is the left eigenvector associated with unity (recall that $\langle\boldsymbol{\pi}|\mathcal{T}=\langle\boldsymbol{\pi}|$), the stationary distribution is the uniform distribution: $\langle\boldsymbol{\pi}| = \frac{1}{6}[1\,1\,1\,1\,1\,1]$, *i.e.*, $\langle\boldsymbol{\pi}| = \frac{1}{6}\langle\mathbf{1}|$, for $\alpha,\beta\in(0,1)$. Hence, throughout this range, the projection operator associated with unity is $\mathcal{T}_1 = \frac{1}{6}|\mathbf{1}\rangle\langle\mathbf{1}|$.

It is interesting to note that the eigenvalue of $1-2\beta$ is associated with the decay of out-of-equilibrium probability density between the Hägg states of $\mathcal{U}$ and $\mathcal{V}$ – or at least between the ABC-state clusters into which each of the Hägg states have split. Indeed, from the Hägg-machine: $\Lambda_{\mathsf{T}} = \{1, 1-2\beta\}$. So, questions about the relative occupations of the Hägg states themselves are questions invoking the $1-2\beta$ projection operator. However, due to the antisymmetry of output orientations emitted from each of these Hägg states, the $1-2\beta$ eigenvalue will not make any direct contribution towards answering questions about the process's output statistics. Specifically, $\langle\mathcal{T}^{\xi(\mathcal{A})}_{1-2\beta}\rangle = 0$ for all $\xi\in\{\mathrm{c},\mathrm{a},\mathrm{s}\}$. Since $a_{1-2\beta}=1$, the projection operator is simply the matrix product of the right and left eigenvectors associated with $1-2\beta$. With proper normalization, we have

$$\mathcal{T}_{1-2\beta} = \tfrac{1}{6}|\mathbf{1}-\mathbf{2\beta}\rangle\langle\mathbf{1}-\mathbf{2\beta}|$$

with $|\mathbf{1}-\mathbf{2\beta}\rangle = [1\,1\,1\,-1\,-1\,-1]^{\mathsf{T}}$ and $\langle\mathbf{1}-\mathbf{2\beta}| = [1\,1\,1\,-1\,-1\,-1]$ where T denotes matrix transposition. Then, one can easily check *via* equation (25) that indeed $\langle\mathcal{T}^{\xi(\mathcal{A})}_{1-2\beta}\rangle = 0$ for all $\xi\in\{\mathrm{c},\mathrm{a},\mathrm{s}\}$.

To obtain an explicit expression for the CFs, we must obtain the remaining projection operators. We can always use equation (19). However, to draw attention to useful techniques, we will break the remaining analysis into two parts: one for $\sigma=0$ and the other for $\sigma\neq0$. In particular, for the case of $\sigma=0$, we show that nondiagonalizablity need not make the problem harder than the diagonalizable case.

5.2.1. $\sigma = 0$. As mentioned earlier, the $\sigma=0$ line is the critical line that organizes a phase transition in the ML ordering. We also find that $\mathcal{T}$ is nondiagonalizable only along the $\sigma=0$ submanifold. For $\sigma=0$, the $\frac{1}{2}(1-\beta)\pm\frac{1}{2}\sigma^{1/2}$ eigenvalues of equation (36) collapse to a single eigenvalue so that the set of eigenvalues reduces to $\Lambda_{\mathcal{T}}|_{\sigma=0} = \{1, 1-2\beta, -\frac{1}{2}(1-\beta)\}$ with corresponding indices $\nu_1=1$, $\nu_{1-2\beta}=1$ and $\nu_{-\overline{\beta}/2}=2$.

In this case, the projection operators are simple to obtain. As in the general case, we have

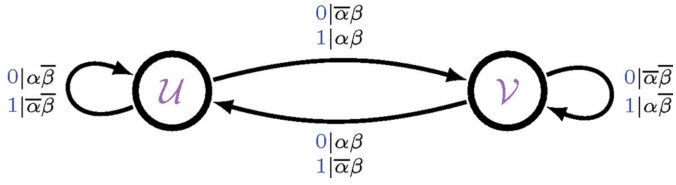

Figure 8
RGDF process, first proposed by Estevez-Rams *et al.* (2008) and adapted here from panel (*c*) of their Fig. 2. There is a slight change in notation. We relabeled the states given as 'f' and 'b' by Estevez-Rams *et al.* (2008) as '$\mathcal{U}$' and '$\mathcal{V}$' and, instead of drawing an arc for each of the possible eight transitions, we took advantage of the multiple transitions between the same states and labeled each arc with two transitions. There is, of course, no change in meaning; this instead provides for slightly tidier illustration. Additionally, we correct a typographical error in Estevez-Rams *et al.* (2008) when we relabel the transition $\mathrm{b}\xrightarrow{0|\overline{\alpha}\beta}\mathrm{b}$ with $\mathcal{V}\xrightarrow{0|\overline{\alpha}\overline{\beta}}\mathcal{V}$.

$$\mathcal{T}_1 = \frac{1}{6}|\mathbf{1}\rangle\langle\mathbf{1}| = \frac{1}{6}\begin{bmatrix} 1 & 1 & 1 & 1 & 1 & 1 \\ 1 & 1 & 1 & 1 & 1 & 1 \\ 1 & 1 & 1 & 1 & 1 & 1 \\ 1 & 1 & 1 & 1 & 1 & 1 \\ 1 & 1 & 1 & 1 & 1 & 1 \\ 1 & 1 & 1 & 1 & 1 & 1 \end{bmatrix}$$

and

$$\mathcal{T}_{1-2\beta} = \frac{1}{6}|\mathbf{1}-2\boldsymbol{\beta}\rangle\langle\mathbf{1}-2\boldsymbol{\beta}| = \frac{1}{6}\begin{bmatrix} 1 & 1 & 1 & -1 & -1 & -1 \\ 1 & 1 & 1 & -1 & -1 & -1 \\ 1 & 1 & 1 & -1 & -1 & -1 \\ -1 & -1 & -1 & 1 & 1 & 1 \\ -1 & -1 & -1 & 1 & 1 & 1 \\ -1 & -1 & -1 & 1 & 1 & 1 \end{bmatrix}.$$

Recall that the projection operators sum to the identity: $\mathbb{I} = \sum_{\lambda\in\Lambda_\mathcal{T}} \mathcal{T}_\lambda = \mathcal{T}_1 + \mathcal{T}_{1-2\beta} + \mathcal{T}_{-\overline{\beta}/2}$. And so, it is easy to obtain the remaining projection operator:

$$\mathcal{T}_{-\overline{\beta}/2} = \mathbb{I} - \mathcal{T}_1 - \mathcal{T}_{1-2\beta} = \frac{1}{3}\begin{bmatrix} 2 & -1 & -1 & 0 & 0 & 0 \\ -1 & 2 & -1 & 0 & 0 & 0 \\ -1 & -1 & 2 & 0 & 0 & 0 \\ 0 & 0 & 0 & 2 & -1 & -1 \\ 0 & 0 & 0 & -1 & 2 & -1 \\ 0 & 0 & 0 & -1 & -1 & 2 \end{bmatrix}.$$

Note that $3\langle\boldsymbol{\pi}|\mathcal{T}^{[A]} = \frac{1}{2}\langle\mathbf{1}|\mathcal{T}^{[A]} = \frac{1}{2}[1\,0\,0\,1\,0\,0]$ and that

$$\mathcal{T}^{[A]}|\mathbf{1}\rangle = \begin{bmatrix} 0 \\ \alpha\overline{\beta}+\overline{\alpha}\beta \\ \alpha\beta+\overline{\alpha}\overline{\beta} \\ 0 \\ \alpha\beta+\overline{\alpha}\overline{\beta} \\ \alpha\overline{\beta}+\overline{\alpha}\beta \end{bmatrix},\quad \mathcal{T}^{[B]}|\mathbf{1}\rangle = \begin{bmatrix} \alpha\beta+\overline{\alpha}\overline{\beta} \\ 0 \\ \alpha\overline{\beta}+\overline{\alpha}\beta \\ \alpha\beta+\overline{\alpha}\overline{\beta} \\ 0 \\ \alpha\overline{\beta}+\overline{\alpha}\beta \end{bmatrix}$$

$$\text{and } \mathcal{T}^{[C]}|\mathbf{1}\rangle = \begin{bmatrix} \alpha\overline{\beta}+\overline{\alpha}\beta \\ \alpha\beta+\overline{\alpha}\overline{\beta} \\ 0 \\ \alpha\beta+\overline{\alpha}\overline{\beta} \\ \alpha\overline{\beta}+\overline{\alpha}\beta \\ 0 \end{bmatrix}.$$

Then, according to equation (20), with $\langle\mathcal{T}_1^{\xi(\mathcal{A})}\rangle = \frac{1}{3}$, $\langle\mathcal{T}_{1-2\beta}^{\xi(\mathcal{A})}\rangle = 0$, $\langle\mathcal{T}_{-\overline{\beta}/2}^{\mathrm{s}(\mathcal{A})}\rangle = -\frac{1}{3}$, $\langle\mathcal{T}_{-\overline{\beta}/2}^{\mathrm{c}(\mathcal{A})}\rangle = \langle\mathcal{T}_{-\overline{\beta}/2}^{\mathrm{a}(\mathcal{A})}\rangle = \frac{1}{6}$, $\langle\mathcal{T}_{-\overline{\beta}/2,1}^{\mathrm{s}(\mathcal{A})}\rangle = \frac{1}{6}(\sigma+\beta-\beta^2) = \frac{1}{6}\beta\overline{\beta}$ and $\langle\mathcal{T}_{-\overline{\beta}/2,1}^{\mathrm{c}(\mathcal{A})}\rangle = \langle\mathcal{T}_{-\overline{\beta}/2,1}^{\mathrm{a}(\mathcal{A})}\rangle = -\frac{1}{12}(\sigma+\beta-\beta^2) = -\frac{1}{12}\beta\overline{\beta}$, the CFs are

$$Q_\xi(n) = \sum_{\lambda\in\Lambda_\mathcal{T}}\sum_{m=0}^{\nu_\lambda-1}\left\langle\mathcal{T}_{\lambda,m}^{\xi(\mathcal{A})}\right\rangle\binom{n-1}{m}\lambda^{n-m-1} = \left\langle\mathcal{T}_1^{\xi(\mathcal{A})}\right\rangle + \sum_{m=0}^{1}\left\langle\mathcal{T}_{-\overline{\beta}/2,m}^{\xi(\mathcal{A})}\right\rangle\binom{n-1}{m}(-\overline{\beta}/2)^{n-m-1} = \frac{1}{3} + \left[\left\langle\mathcal{T}_{-\overline{\beta}/2}^{\xi(\mathcal{A})}\right\rangle - \frac{2}{\overline{\beta}}\left\langle\mathcal{T}_{-\overline{\beta}/2,1}^{\xi(\mathcal{A})}\right\rangle(n-1)\right](-\overline{\beta}/2)^{n-1}.$$

Specifically

$$Q_\mathrm{s}(n) = \frac{1}{3}\left[1 + 2\left(1+\frac{\beta}{\overline{\beta}}n\right)(-\overline{\beta}/2)^n\right] \tag{39}$$

and

$$Q_\mathrm{c}(n) = Q_\mathrm{a}(n) = \frac{1}{3}\left[1 - \left(1+\frac{\beta}{\overline{\beta}}n\right)(-\overline{\beta}/2)^n\right]. \tag{40}$$

5.2.2. $\sigma \neq 0$. For any value of σ, we can obtain the projection operators *via* equation (19). In addition to those quoted above and, in terms of the former $\mathcal{T}_{-\overline{\beta}/2}$, the remaining projection operators turn out to be

$$\mathcal{T}_{\frac{-\overline{\beta}\pm\sigma^{1/2}}{2}} = \pm\frac{1}{\sigma^{1/2}}\mathcal{T}_{-\overline{\beta}/2}\left[\mathcal{T} + \left(\frac{\overline{\beta}\pm\sigma^{1/2}}{2}\right)\mathbb{I}\right].$$

Since the $1-2\beta$ eigen-contribution is null and since

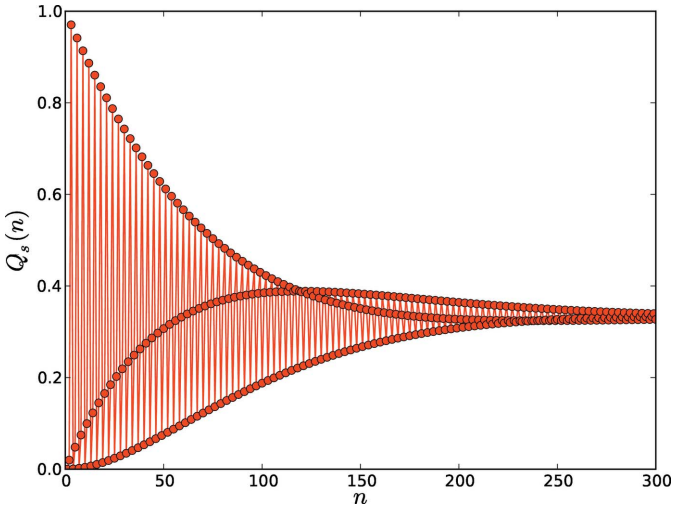

Figure 9
$Q_\mathrm{s}(n)$ *versus* n with $\alpha = 0.01$ and $\beta = 0$ for the RGDF process. This should be compared to panel (*b*) of Fig. 8 in Estevez-Rams *et al.* (2008). Although different means were used to make the calculations, they appear to be identical.

$$\langle T_1^{\xi(\mathcal{A})}\rangle = \frac{1}{3},$$
$$\left\langle T^{\mathrm{s}(\mathcal{A})}_{\frac{-\overline{\beta}\pm\sigma^{1/2}}{2}}\right\rangle = \frac{1}{6}\left[-1 \pm \left(\sigma^{1/2} + \frac{\beta\overline{\beta}}{\sigma^{1/2}}\right)\right]$$
$$= \pm\frac{1}{6}\left(1 \mp \frac{\beta}{\sigma^{1/2}}\right)(\sigma^{1/2} \mp \overline{\beta}) \text{ and}$$
$$\left\langle T^{\mathrm{c}(\mathcal{A})}_{\frac{-\overline{\beta}\pm\sigma^{1/2}}{2}}\right\rangle = \left\langle T^{\mathrm{a}(\mathcal{A})}_{\frac{-\overline{\beta}\pm\sigma^{1/2}}{2}}\right\rangle$$
$$= \frac{1}{12}\left[1 \mp \left(\sigma^{1/2} + \frac{\beta\overline{\beta}}{\sigma^{1/2}}\right)\right]$$
$$= \mp\frac{1}{12}\left(1 \mp \frac{\beta}{\sigma^{1/2}}\right)(\sigma^{1/2} \mp \overline{\beta}),$$

the CFs for $\sigma \neq 0$ are

$$Q_\xi(n) = \sum_{\lambda\in\Lambda_\mathcal{T}} \lambda^{n-1} \sum_{x_0\in\mathcal{A}_\mathrm{P}} \langle\boldsymbol{\pi}|\mathcal{T}^{[x_0]}\mathcal{T}_\lambda\mathcal{T}^{[\hat{\xi}(x_0)]}|\mathbf{1}\rangle$$
$$= \frac{1}{3} + \sum_{\lambda\in\{\frac{-\overline{\beta}\pm\sigma^{1/2}}{2}\}} \left\langle T_\lambda^{\xi(\mathcal{A})}\right\rangle \lambda^{n-1}. \tag{41}$$

Specifically, for $\xi = \mathrm{s}$

$$Q_\mathrm{s}(n) = \frac{1}{3} + \frac{1}{6}\left(1 - \frac{\beta}{\sigma^{1/2}}\right)(\sigma^{1/2} - \overline{\beta})\left(\frac{-\overline{\beta} + \sigma^{1/2}}{2}\right)^{n-1}$$
$$- \frac{1}{6}\left(1 + \frac{\beta}{\sigma^{1/2}}\right)(\sigma^{1/2} + \overline{\beta})\left(\frac{-\overline{\beta} - \sigma^{1/2}}{2}\right)^{n-1}$$
$$= \frac{1}{3}\left[1 + \left(1 - \frac{\beta}{\sigma^{1/2}}\right)\left(\frac{-\overline{\beta} + \sigma^{1/2}}{2}\right)^{n} + \left(1 + \frac{\beta}{\sigma^{1/2}}\right)\left(\frac{-\overline{\beta} - \sigma^{1/2}}{2}\right)^{n}\right], \tag{42}$$

and we recover equation (29) of Estevez-Rams *et al.* (2008).

Estevez-Rams *et al.* (2008) recount the embarrassingly long list of recent failures of previous attempts to analyze organization in RGDF-like processes. These failures resulted from not obtaining all of the terms in the CFs, which in turn stem primarily from not using a sufficiently clever ansatz in their methods, together with not knowing how many terms there should be. In contrast, even when casually observing the number of HMM states, our method gives immediate knowledge of the number of terms. Our method is generally applicable with straightforward steps to actually calculate all the terms once and for all.

Figs. 9, 10, 11 and 12 show plots of $Q_\mathrm{s}(n)$ *versus* n for the RGDF process at different values of α and β. The first two graphs, Figs. 9 and 10, were previously produced by Estevez-Rams *et al.* (2008) and appear to be identical to our results. The second pair of graphs for the RGDF process, Figs. 11 and 12, show the behavior of the CFs for larger values of α and β, but with the numerical values of each exchanged ($0.1 \Leftrightarrow 0.2$). The CFs are clearly sensitive to the kind of faulting present, as one would expect. However, each does decay to 1/3, as they must.

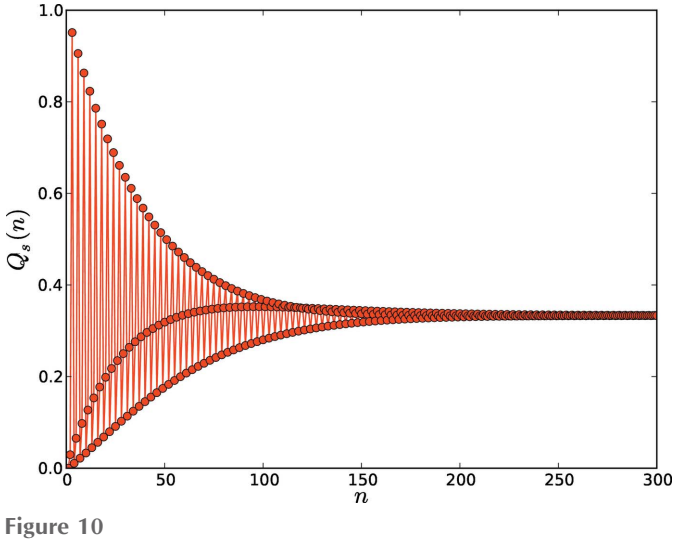

Figure 10
$Q_\mathrm{s}(n)$ *versus* n with $\alpha = 0.01$ and $\beta = 0.01$ for the RGDF process. Comparison with panel (*d*) of Fig. 8 in Estevez-Rams *et al.* (2008) shows an identical result.

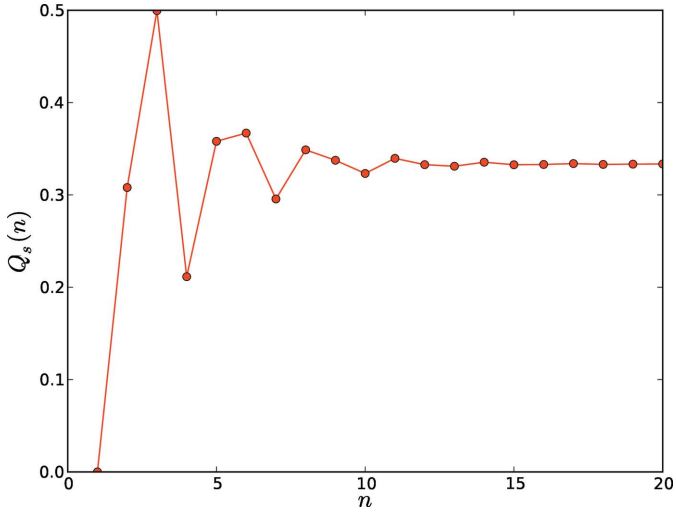

Figure 11
$Q_\mathrm{s}(n)$ *versus* n with $\alpha = 0.1$ and $\beta = 0.2$ for the RGDF process.

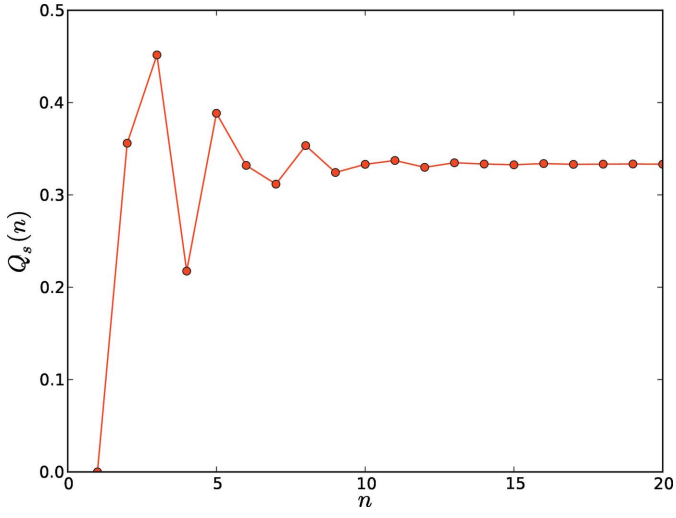

Figure 12
$Q_\mathrm{s}(n)$ *versus* n with $\alpha = 0.2$ and $\beta = 0.1$ for the RGDF process.

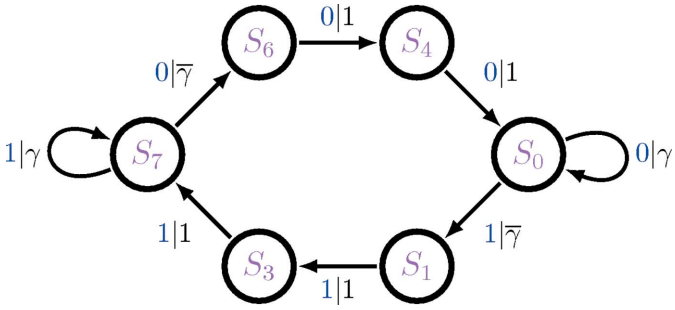

Figure 13
Hägg-machine for the SFSF process, inspired by the observations of Sun *et al.* (2012). We observe that there is one faulting parameter $\gamma \in [0, 1]$ and three SSCs. Or, equivalently three causal-state cycles, as this graph is also an ε-machine. The three SSCs are $[S_7]$, $[S_0]$ and $[S_7S_6S_4S_0S_1S_3]$. The latter we recognize as the 6*H* structure if $\gamma = 0$. For large values of γ, *i.e.*, as $\gamma \to 1$, this process approaches a twinned 3*C* structure, although the faulting is *not* random. The causal-state architecture prevents the occurrence of domains of size-three or less.

5.3. Shockley–Frank stacking faults in 6*H*-SiC: the SFSF process

While promising as a material for next-generation electronic components, fabricating SiC crystals of a specified polytype remains challenging. Recently Sun *et al.* (2012) reported experiments on 6*H*-SiC epilayers (∼200 µm thick) produced by the fast sublimation growth process at 2048 K. Using high-resolution transmission electron microscopy, they were able to survey the kind and amount of particular stacking faults present. In the Hägg notation 6*H*-SiC is specified by 000111, and this is written in the Zhdanov notation as (3,3) (Ortiz *et al.*, 2013). Thus, unfaulted 6*H*-SiC can be thought of as alternating blocks of size-three domains. *Ab initio* super-cell calculations by Iwata *et al.* (2003) predicted that the Shockley defects (4,2), (5,1), (9,3) and (10,2) should be present, with the (4,2) defect having the lowest energy and, thus, it presumably should be the most common. Of these, however, Sun *et al.* (2012) observed only the (9,3) defect [given there as (3,9)] and, at that, only once. Instead, the most commonly observed defects were (3,4), (3,5), (3,6) and (3,7), appearing nine, two, two and three times, respectively, with isolated instances of other stacking-fault sequences. They postulated that combined Shockley–Frank defects (Hirth & Lothe, 1968) could produce these results. The (3,4) stacking sequences could be explained as external Frank stacking faults, and the other observed faults could result from further Shockley defects merging with these (3,4) SFs. We call this process the *Shockley–Frank Stacking Fault* (SFSF) process.

Inspired by these observations, we ask what causal-state structure could produce such stacking sequences. We suggest that the ε-machine shown in Fig. 13 is a potential candidate, with $\gamma \in [0, 1]$ as the sole faulting parameter. (Here, we must insist that only a thorough analysis, with significantly more data, such as that obtainable from high-resolution transmission electron microscopy or a diffraction pattern, can properly reveal the appropriate causal-state structure. The SFSF process is given primarily to illustrate our methods.) For weakly faulted crystals ($\gamma \simeq 0$), as seems to be the case here, there must be a causal-state cycle that gives the 6*H* structure, and we see that the causal-state sequence $[S_7S_6S_4S_0S_1S_3]$ does that. Indeed, if the fault parameter γ were identically zero, then this ε-machine would give only the 6*H* structure. Sun *et al.* (2012)'s observations suggest that deviations from 6*H* structure occur (almost) always as *additions* to the size-three 0 or 1 domains. The self-state transitions on S_7 and S_0 have just this effect: after seeing three consecutive 1's (0's), with probability γ, the current domain will increase in size to four. And, likewise, with probability γ, size-four domains will increase to size-five domains. Thus, with decreasing probability, the faults (3,4), (3,5) ... can be modeled by this ε-machine. Notice that the causal architecture prevents domains of any size less than three, which is consistent with the bulk of the observations by Sun *et al.* (2012).[14] Also, this ε-machine does predict (4,4) sequences, which Sun *et al.* (2012) observed once. Thus, qualitatively, and approximately quantitatively, the proposed ε-machine largely reproduces the observations of Sun *et al.* (2012).

We begin by identifying the SSCs on the HMM, the ε-machine shown in Fig. 13. We find that there are three, $[S_7]$, $[S_0]$ and $[S_7S_6S_4S_0S_1S_3]$. We calculate the winding numbers to be $W^{[S_7]} = 1$, $W^{[S_0]} = -1$ and $W^{[S_7S_6S_4S_0S_1S_3]} = 0$. The first two of these SSCs vanish if $\gamma = 0$, giving a nonmixing Hägg-machine. Thus, for $\gamma \neq 0$ the Hägg-machine is mixing and we proceed with the case of $\gamma \in (0, 1]$.

By inspection we write down the two 6-by-6 TMs of the Hägg-machine as

$$\mathsf{T}^{[0]} = \begin{bmatrix} \gamma & 0 & 0 & 0 & 0 & 0 \\ 0 & 0 & 0 & 0 & 0 & 0 \\ 0 & 0 & 0 & 0 & 0 & 0 \\ 0 & 0 & 0 & 0 & \overline{\gamma} & 0 \\ 0 & 0 & 0 & 0 & 0 & 1 \\ 1 & 0 & 0 & 0 & 0 & 0 \end{bmatrix}$$

and

$$\mathsf{T}^{[1]} = \begin{bmatrix} 0 & \overline{\gamma} & 0 & 0 & 0 & 0 \\ 0 & 0 & 1 & 0 & 0 & 0 \\ 0 & 0 & 0 & 1 & 0 & 0 \\ 0 & 0 & 0 & \gamma & 0 & 0 \\ 0 & 0 & 0 & 0 & 0 & 0 \\ 0 & 0 & 0 & 0 & 0 & 0 \end{bmatrix},$$

where the states are ordered S_0, S_1, S_3, S_7, S_6 and S_4. The internal-state TM is their sum:

[14] They did observe a single (3,2) sequence (see their Table I), and the SFSF process cannot reproduce that structure. Additional causal states and/or transitions would be needed to accommodate this additional stacking structure. One obvious and simple modification that would produce domains of size two would be to allow the transitions $S_3 \xrightarrow{0} S_6$ and $S_4 \xrightarrow{1} S_1$ with some small probability. However, in the interest of maintaining a reasonably clear example, we neglect this possibility.

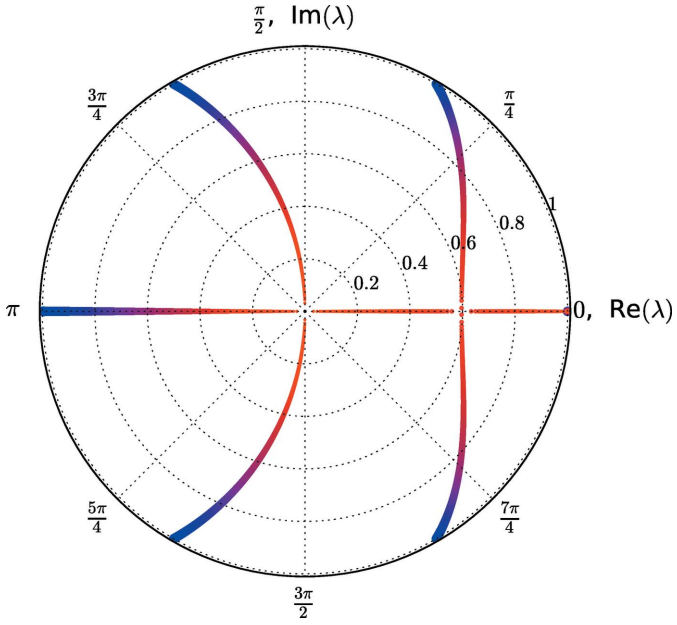

Figure 14
The six eigenvalues of the Hägg-machine as they evolve from $\gamma = 0$ (thickest blue markings) to $\gamma = 1$ (thinnest red markings). Note that the eigenvalues at $\gamma = 0$ are the six roots of unity. Unity is a persistent eigenvalue. Four of the eigenvalues approach 0 as $\gamma \rightarrow 1$. Another of the eigenvalues approaches unity as $\gamma \rightarrow 1$. The eigenvalues are nondegenerate throughout the parameter range except for the transformation event where the two eigenvalues on the right collide and scatter upon losing their imaginary parts.

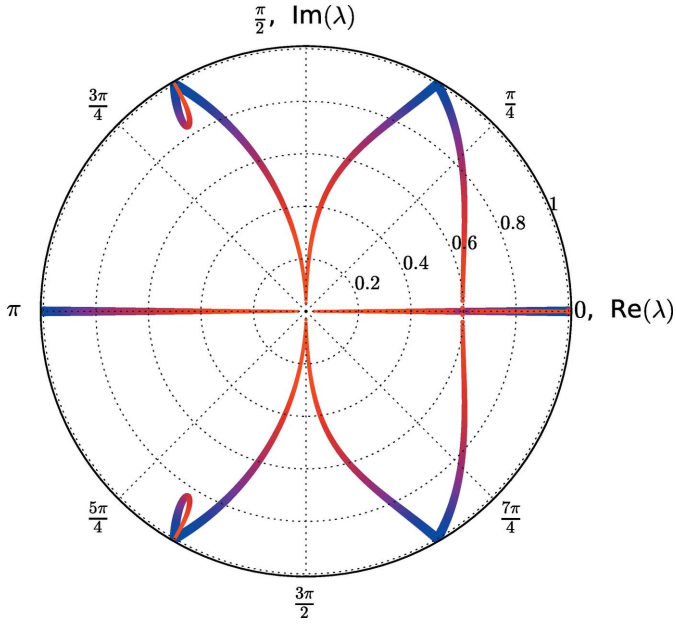

Figure 15
The 18 eigenvalues of the *ABC*-machine as they evolve from $\gamma = 0$ (thickest blue markings) to $\gamma = 1$ (thinnest red markings). Note that the eigenvalues at $\gamma = 0$ are still the six roots of unity. The new eigenvalues introduced *via* transformation to the *ABC*-machine all appear in degenerate (but diagonalizable) pairs. In terms of increasing γ, these include eigenvalues approaching zero from ± 1, eigenvalues taking a left branch towards zero as they lose their imaginary parts, and eigenvalues looping away and back towards the nontrivial cube roots of unity.

$$\mathsf{T} = \begin{bmatrix} \gamma & \overline{\gamma} & 0 & 0 & 0 & 0 \\ 0 & 0 & 1 & 0 & 0 & 0 \\ 0 & 0 & 0 & 1 & 0 & 0 \\ 0 & 0 & 0 & \gamma & \overline{\gamma} & 0 \\ 0 & 0 & 0 & 0 & 0 & 1 \\ 1 & 0 & 0 & 0 & 0 & 0 \end{bmatrix}.$$

Since the six-state Hägg-machine generates an $(3 \times 6 =)$ 18-state *ABC*-machine, we do not explicitly write out the TMs of the *ABC*-machine. Nevertheless, it is straightforward to expand the Hägg-machine to the *ABC*-machine *via* the rote expansion method of §3.3. It is also straightforward to apply equation (15) to obtain the CFs as a function of the faulting parameter γ. To use equation (15), note that the stationary distribution over the *ABC*-machine can be obtained *via* equation (9) with

$$\langle \boldsymbol{\pi}_{\mathrm{H}}| = \frac{1}{6 - 4\gamma}[1 \ \overline{\gamma} \ \overline{\gamma} \ 1 \ \overline{\gamma} \ \overline{\gamma}]$$

as the stationary distribution over the Hägg-machine.

The eigenvalues of the Hägg TM can be obtained as the solutions of $\det(\mathsf{T} - \lambda\mathbb{I}) = (\lambda - \gamma)^2\lambda^4 - \overline{\gamma}^2 = 0$. These include 1, $-\frac{1}{2}\overline{\gamma} \pm (\gamma^2 + 2\gamma - 3)^{1/2}$, and three other eigenvalues involving cube roots. Their values are plotted in the complex plane in Fig. 14 as we sweep through γ.

The eigenvalues of the *ABC* TM are similarly obtained as the solutions of $\det(\mathcal{T} - \lambda\mathbb{I}) = 0$. The real and imaginary parts of these eigenvalues are plotted in Fig. 15. Note that $\Lambda_{\mathcal{T}}$ inherits Λ_{T} as the backbone for its more complex structure, just as $\Lambda_{\mathsf{T}} \subseteq \Lambda_{\mathcal{T}}$ for all of our previous examples. The eigenvalues in $\Lambda_{\mathcal{T}}$ are, of course, those most directly responsible for the structure of the CFs.

The SFSF process's CFs are shown for several example parameter values of γ in Figs. 16, 17, 18 and 19 calculated directly from numerical implementation of equation (15). As the faulting parameter is increased from $0.01 \rightarrow 0.5$, the CFs

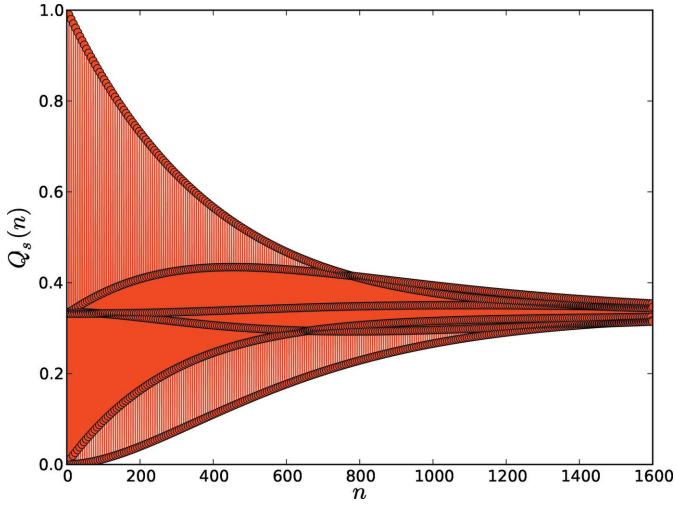

Figure 16
$Q_s(n)$ *versus* n for the SFSF process with $\gamma = 0.01$. This specimen is only very weakly faulted and, hence, there are small decay constants giving a slow decay to 1/3.

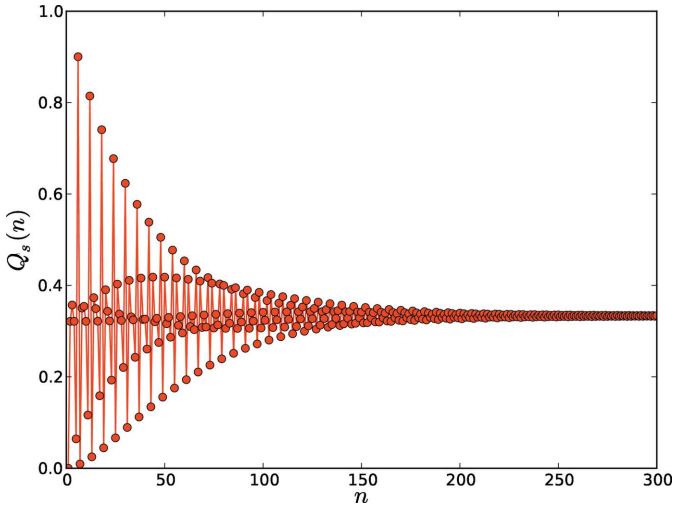

Figure 17
$Q_s(n)$ *versus* n for the SFSF process with $\gamma = 0.1$. With increasing γ, the CFs approach their asymptotic value of 1/3 much more quickly.

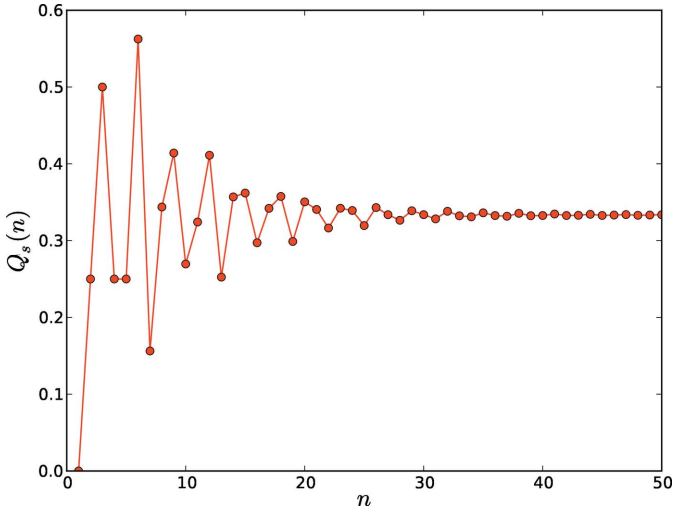

Figure 18
$Q_s(n)$ *versus* n for the SFSF process with $\gamma = 0.5$. Here, the specimen is quite disordered, and the CFs decay quickly.

begin to decay more quickly. However, for $\gamma = 0.9$, the correlation length increases as the eigenvalues, near the nontrivial cube roots of unity, loop back towards the unit circle. The behavior near $\gamma = 0.9$ suggests a longer-ranged and more regularly structured specimen, even though there are fewer significant eigen-contributions to the specimen's structure. Indeed, the bulk of the structure is now more apparent but less sophisticated.

6. Conclusion

We introduced a new approach to exactly determining CFs directly from HMMs that describe layered CPSs. The calculation can be done either with high numerical accuracy and efficiency, as we have shown in the CF plots for each example, or analytically, as was done for the IID and RGDF processes.

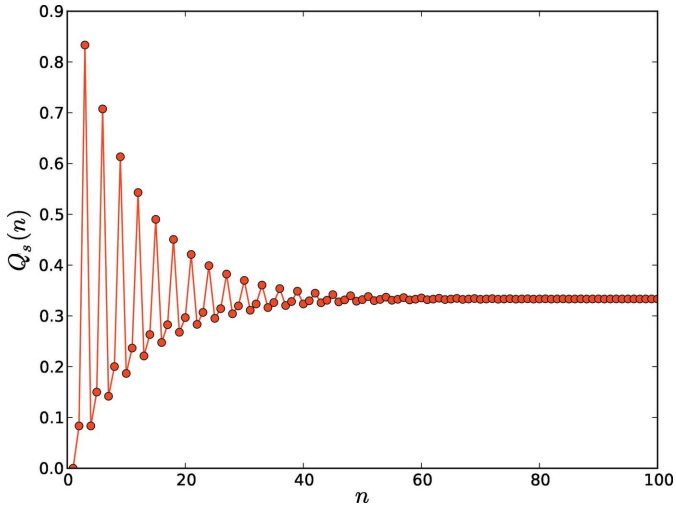

Figure 19
$Q_s(n)$ *versus* n for the SFSF process with $\gamma = 0.9$. The slower CF decay suggests that the process is now less disordered than the $\gamma = 0.5$ case. Notice that this CF is large for $n \bmod (3) = 0$, indicating strong correlation between MLs separated by a multiple of three MLs. This is the kind of behavior that one expects from a twinned 3*C* crystal.

The mathematical object that assumes central importance here is the HMM. While we appreciate the value that studying CFs and, more generally, pair distribution functions brings to understanding material structure, pairwise correlation information is better thought of as a consequence of a more fundamental entity (*i.e.*, the HMM) than one of intrinsic importance. This becomes clear when we consider that the structure is completely contained in the very compact HMM representation. More to the point, all of the correlation information is directly calculable from it, as we demonstrated. In contrast, the task of inverting correlation information to specify the underlying organization of a material's structure, *i.e.*, its HMM, is highly nontrivial. Over the past century considerable effort has been expended to invert diffraction patterns, the Fourier transform of the CFs, into these compact structural models.[15] The work of Warren (1969), Krishna and coworkers (Sebastian & Krishna, 1984; Sebastian & Krishna, 1987*a*,*b*,*c*; Sebastian *et al.*, 1987), Berliner & Werner (1986) and that of our own group (Varn *et al.*, 2002, 2007, 2013*a*,*b*), to mention a few, all stand in testament to this effort.

Although the presentation concentrated on CFs in layered CPSs, the potential impact of the new approach is far wider. First, we note that it was necessary to make several assumptions about the geometry of the stacking process, *i.e.*, the number of possible orientations of each ML and how two MLs can be stacked, in order to demonstrate numerical results and make contact with previous work. These assumptions however in no way limit the applicability: any set of stacking rules over a finite number of possible positions is amenable to this treatment. Second, it may seem that starting with a HMM is unnecessarily restrictive. It is not. Given a sample of the

[15] We have not explicitly made the connection here, but almost all previous models of planar disorder can generically be expressed as HMMs.

stacking process from (say) a simulation study, there are techniques that now have become standard for finding the ε-machine, a kind of HMM, that describes the process. The subtree-merging method (Crutchfield & Young, 1989) and causal-state splitting reconstruction (Shalizi *et al.*, 2002) are perhaps the best known, but recently a new procedure based on Bayesian inference has been developed (Strelioff & Crutchfield, 2014). Finally, a HMM may be proposed on theoretical grounds, as done with the RGDF and SFSF HMMs in our second and third examples. And, for the case when a diffraction pattern is available, there is ε-machine spectral reconstruction theory (Varn *et al.*, 2002, 2007, 2013*a*,*b*). We anticipate that HMMs will become the standard representation for describing layered structures.

The approach presented here should also be viewed in the larger context of our recent research thrusts. While crystallography has historically struggled to settle on a formalism to describe disordered structures, we propose that such a framework has been identified, at least for layered materials. Based in computational mechanics, *chaotic crystallography* (Varn & Crutchfield, 2015) employs information theory as a key component to characterize disordered materials. Although the use of information theory in crystallography has been previously proposed by Mackay and coworkers (Mackay, 1986, 2002; Cartwright & Mackay, 2012), chaotic crystallography realizes this goal. Additionally, using spectral methods in the spirit of §4.2, information- and computation-theoretic measures are now directly calculable from ε-machines (Crutchfield *et al.*, 2013; Riechers & Crutchfield, 2015). And importantly, a sequel will demonstrate how spectral methods can give both a fast and efficient method for calculating the diffraction pattern of layered CPSs or analytical expressions thereof (Riechers *et al.*, 2014).

APPENDIX *A*
Transition matrices, projection operators and bra–ket notation

The substochastic symbol-labeled transition matrices of a HMM sum to give our probability-conserving right-stochastic (*i.e.*, all rows sum to one) state-to-state transition matrix $\mathcal{T} = \sum_{x\in\mathcal{A}} \mathcal{T}^{[x]}$. All eigenvalues of this matrix lie on or within the unit circle in the complex plane. We use a bra–ket notation to easily identify bras $\langle\cdot|$ as row vectors and kets $|\cdot\rangle$ as column vectors. A special set of kets are right eigenvectors of $\mathcal{T}$. The right eigenvectors satisfy

$$\mathcal{T}|\lambda\rangle = \lambda|\lambda\rangle$$

for $\lambda \in \Lambda_{\mathcal{T}}$. A corresponding set of bras are left eigenvectors of $\mathcal{T}$. The left eigenvectors satisfy

$$\langle\lambda|\mathcal{T} = \lambda\langle\lambda|$$

for $\lambda \in \Lambda_{\mathcal{T}}$. In general, unlike the special case in quantum mechanics, the left eigenvectors are not merely the conjugate transpose of the right eigenvectors. Projection operators play a prominent role in the development of our results. For the general case, they can be obtained from equation (19). However, in the simplest case of a projection operator of a nondegenerate eigenvalue, the projection operator can simply be expressed as

$$\mathcal{T}_\lambda = \frac{1}{\langle\lambda|\lambda\rangle}|\lambda\rangle\langle\lambda|,$$

where the denominator is simply a normalizing factor. The only normalization convention we impose is that $|\mathbf{1}\rangle$ represents the right eigenvector associated with unity of all ones and $\langle\boldsymbol{\pi}|$ is the left eigenvector associated with unity normalized in probability. This normalization allows $\mathcal{T}_1 = |\mathbf{1}\rangle\langle\boldsymbol{\pi}|$ and consistent interpretation of unconditioned probabilities: $\Pr(w) = \langle\boldsymbol{\pi}|\mathcal{T}^{[w]}|\mathbf{1}\rangle$. Further useful results and discussion of the mathematical machinery can be found in Riechers & Crutchfield (2015).

Acknowledgements

The authors thank the Santa Fe Institute for its hospitality during visits. JPC is an External Faculty member there. This material is based upon work supported by, or in part by, the US Army Research Laboratory and the US Army Research Office under contracts W911NF-12-1-0234 and W911NF-13-1-0390.

References

Ashcroft, N. W. & Mermin, N. D. (1976). *Solid State Physics*. New York: Saunders College Publishing.
Berliner, R. & Werner, S. (1986). *Phys. Rev. B*, **34**, 3586–3603.
Beyerlein, K. R., Snyder, R. L. & Scardi, P. (2011). *Acta Cryst.* A**67**, 252–263.
Cartwright, J. H. E. & Mackay, A. L. (2012). *Philos. Trans. R. Soc. A*, **370**, 2807–2822.
Castro Neto, A. H., Guinea, F., Peres, N. M. R., Novoselov, K. S. & Geim, A. K. (2009). *Rev. Mod. Phys.* **81**, 109–162.
Cliffe, M. J., Dove, M. T., Drabold, D. A. & Goodwin, A. L. (2010). *Phys. Rev. Lett.* **104**, 125501.
Cover, T. M. & Thomas, J. A. (2006). *Elements of Information Theory*, 2nd ed. Hoboken: John Wiley and Sons.
Crutchfield, J. P. (2012). *Nature Phys.* **8**, 17–24.
Crutchfield, J. P., Ellison, C. J. & Riechers, P. M. (2013). ArXiv 1309.3792.
Crutchfield, J. P. & Feldman, D. P. (2003). *Chaos*, **13**, 25–54.
Crutchfield, J. P. & Young, K. (1989). *Phys. Rev. Lett.* **63**, 105–108.
Dornberger-Schiff, K. & Schmittler, H. (1971). *Acta Cryst.* A**27**, 216–219.
Egami, T. & Billinge, S. J. L. (2013). *Underneath the Bragg Peaks: Structural Analysis of Complex Materials*, Vol. 16, 2nd ed. *Pergamon Materials Series*. New York: Pergamon.
Elliot, R. J., Aggoun, L. & Moore, J. B. (1995). *Hidden Markov Models: Estimation and Control*, Vol. 29 of *Applications of Mathematics*. New York: Springer.
Ellison, C. J., Mahoney, J. R. & Crutchfield, J. P. (2009). *J. Stat. Phys.* **136**, 1005–1034.
Ephraim, Y. & Merhav, N. (2002). *IEEE Trans. Inf. Theory*, **48**, 1518–1569.
Estevez-Rams, E., Martinez, J., Penton-Madrigual, A. & Lora-Serrano, R. (2001). *Phys. Rev. B*, **63**, 054109.
Estevez-Rams, E., Penton-Madrigal, A., Lora-Serrano, R. & Martinez-Garcia, J. (2001). *J. Appl. Cryst.* **34**, 730–736.
Estevez-Rams, E., Welzel, U., Pentón Madrigal, A. & Mittemeijer, E. J. (2008). *Acta Cryst.* A**64**, 537–548.

Ferraris, G., Makovicky, E. & Merlino, S. (2008). *Crystallography of Modular Materials*, Vol. 15 of *International Union of Crystallography Monographs on Crystallography*. Oxford: Oxford University Press.
Geim, A. K. & Grigorieva, I. V. (2013). *Nature (London)*, **499**, 419–425.
Guinier, A. (1963). *X-Ray Diffraction in Crystals, Imperfect Crystals and Amorphous Bodies.* New York: W. H. Freeman and Company.
Hendricks, S. & Teller, E. (1942). *J. Chem. Phys.* **10**, 147–167.
Hirth, J. P. & Lothe, J. (1968). *Theory of Dislocations*, 2nd ed. New York: McGraw-Hill.
Hopcroft, J. E. & Ullman, J. D. (1979). *Introduction to Automata Theory, Languages and Computation*. Reading: Addison-Wesley.
Iwata, H. P., Lindefelt, U., Öberg, S. & Briddon, P. R. (2003). *J. Appl. Phys.* **94**, 4972–4979.
Kabra, V. K. & Pandey, D. (1988). *Phys. Rev. Lett.* **61**, 1493–1496.
Kabra, V. K. & Pandey, D. (1995). *Acta Cryst.* A**51**, 329–335.
Karlin, S. & Taylor, H. M. (1975). *A First Course in Stochastic Processes*, 2nd ed. New York: Academic Press.
Mackay, A. L. (1986). *Comput. Math. Appl.* B**12**, 21–37.
Mackay, A. L. (2002). *Struct. Chem.* **13**, 215–220.
Oppenheim, A. V. & Schafer, R. W. (1975). *Digital Signal Processing.* Englewood Cliffs: Prentice-Hall.
Ortiz, A. L., Sánchez-Bajo, F., Cumbrera, F. L. & Guiberteau, F. (2013). *J. Appl. Cryst.* **46**, 242–247.
Paz, A. (1971). *Introduction to Probabilistic Automata.* New York: Academic Press.
Price, G. D. (1983). *Phys. Chem. Miner.* **10**, 77–83.
Rabiner, L. R. (1989). *IEEE Proc.* **77**, 257.
Riechers, P. M. & Crutchfield, J. P. (2015). In preparation.
Riechers, P. M., Varn, D. P. & Crutchfield, J. P. (2014). ArXiv 1410.5028; Santa Fe Institute Working Paper 14-10-38.
Sebastian, M. T. & Krishna, P. (1984). *Philos. Mag. A*, **49**, 809–821.
Sebastian, M. T. & Krishna, P. (1987*a*). *Phys. Status Solidi (a)*, **101**, 329–337.
Sebastian, M. T. & Krishna, P. (1987*b*). *Cryst. Res. Technol.* **22**, 929–941.
Sebastian, M. T. & Krishna, P. (1987*c*). *Cryst. Res. Technol.* **22**, 1063–1072.
Sebastian, M. T. & Krishna, P. (1994). *Random, Non-Random and Periodic Faulting in Crystals.* The Netherlands: Gordon and Breach.
Sebastian, M. T., Narayanan, K. & Krishna, P. (1987). *Phys. Status Solidi (a)*, **102**, 241–249.
Shalizi, C. R. & Crutchfield, J. P. (2001). *J. Stat. Phys.* **104**, 817–881.
Shalizi, C. R., Shalizi, K. L. & Crutchfield, J. P. (2002). arXiv.org/abs/cs.LG/0210025; Santa Fe Institute Working Paper, 02-10-060.
Shrestha, S. P. & Pandey, D. (1996*a*). *Europhys. Lett.* **34**, 269–274.
Shrestha, S. P. & Pandey, D. (1996*b*). *Acta Mater.* **44**, 4949–4960.
Shrestha, S. P. & Pandey, D. (1997). *Proc. R. Soc. London Ser. A*, **453**, 1311–1330.
Shrestha, S. P., Tripathi, V., Kabra, V. K. & Pandey, D. (1996). *Acta Mater.* **44**, 4937–4947.
Strelioff, C. C. & Crutchfield, J. P. (2014). *Phys. Rev. E*, **89**, 042119.
Sun, J. W., Robert, T., Andreadou, A., Mantzari, A., Jokubavicius, V., Yakimova, R., Camassel, J., Juillaguet, S., Polychroniadis, E. K. & Syväjärvi, M. (2012). *J. Appl. Phys.* **111**, 113527.
Tiwary, P. & Pandey, D. (2007). *Acta Cryst.* A**63**, 289–296.
Varn, D. P. (2001). PhD thesis, University of Tennessee, Knoxville, USA.
Varn, D. P. & Canright, G. S. (2001). *Acta Cryst.* A**57**, 4–19.
Varn, D. P., Canright, G. S. & Crutchfield, J. P. (2002). *Phys. Rev. B*, **66**, 174110.
Varn, D. P., Canright, G. S. & Crutchfield, J. P. (2007). *Acta Cryst.* B**63**, 169–182.
Varn, D. P., Canright, G. S. & Crutchfield, J. P. (2013*a*). *Acta Cryst.* A**69**, 197–206.
Varn, D. P., Canright, G. S. & Crutchfield, J. P. (2013*b*). *Acta Cryst.* A**69**, 413–426.
Varn, D. P. & Crutchfield, J. P. (2004). *Phys. Lett. A*, **324**, 299–307.
Varn, D. P. & Crutchfield, J. P. (2015). *Curr. Opin. Chem. Eng.* **7**, 47–56.
Warren, B. E. (1969). *X-Ray Diffraction.* Reading, MA: Addison-Wesley.
Wilson, A. J. C. (1942). *Proc. R. Soc. London Ser. A*, **180**, 277–285.
Yi, J. & Canright, G. S. (1996). *Phys. Rev. B*, **53**, 5198–5210.
Zekentes, K. & Rogdakis, K. (2011). *J. Phys. D Appl. Phys.* **44**, 133001.